Reexamination of Tsunami Source Models For the 20th Century Earthquakes Off Hokkaido and Tohoku Along the Eastern Margin of the Sea of Japan

Satoko Murotani (s-muro@kahaku.go.jp)
National Museum of Nature and Science: Kokuritsu Kagaku Hakubutsukan https://orcid.org/0000-0002-8634-5338
Kenji Satake
Earthquake Reserch Institute, The University of Tokyo
Takeo Ishibe
Association for the Development of Earthquake Prediction
Tomoya Harada
Earthquake Research Institute, The University of Tokyo

Full paper

Keywords: Large earthquakes of the Sea of Japan, 1940 off Shakotan Peninsula earthquake, 1993 off the southwest coast of Hokkaido earthquake, 1983 Central Sea of Japan earthquake, 1983 west off Aomori earthquake, 1964 off Oga Peninsula earthquake, Teleseismic waveform inversion, Tsunami numerical simulation, Scaling relation for seismic moment and source area

Posted Date: October 13th, 2021

DOI: https://doi.org/10.21203/rs.3.rs-940165/v1

Abstract

Large earthquakes around Japan occur not only in the Pacific Ocean but also in the Sea of Japan, and cause both damage from the earthquake itself and from the ensuing tsunami to the coastal areas. Recently, offshore active fault surveys were conducted in the Sea of Japan by the Integrated Research Project on Seismic and Tsunami Hazards around the Sea of Japan (JSPJ), and their fault models (length, width, strike, dip, and slip angles) have been obtained. We examined the causative faults of M7 or larger earthquakes in the Sea of Japan during the 20th century using seismic and tsunami data. The 1940 off Shakotan Peninsula earthquake (M_{JMA} 7.5) appears to have been caused by the offshore active faults MS01, MS02, ST01, and ST02 as modelled by the JSPJ. The 1993 off the southwest coast of Hokkaido earthquake (M_{JMA} 7.8) likely occurred on the offshore active faults OK03a, OK03b, and OK05, while the 1983 Central Sea of Japan earthquake (M_{JMA} 7.7) probably related to MMS01, MMS04, and MGM01. For these earthquakes, the observed tsunami waveforms were basically reproduced by tsunami numerical simulation from the offshore active faults with the slip amounts obtained by the scaling relation with three stages between seismic moment and source area for inland earthquakes. However, the observed tsunami runup heights along the coast were not reproduced at certain locations, possibly because of the coarse bathymetry data used for the simulation. The 1983 west off Aomori (M_{JMA} 7.1) and the 1964 off Oga Peninsula (M_{JMA} 6.9) earthquakes showed multiple faults near the source area that could be used to reproduce the observed tsunami waveforms; therefore, we could not identify the causative faults. Further analysis using near-field seismic waveforms is required for their identification of their causative faults and their parameters. The scaling relation for inland earthquakes can be used to obtain the slip amounts for offshore active faults in the Sea of Japan and to estimate the coastal tsunami heights and inundation area which can be useful for disaster prevention and mitigation of future earthquakes and tsunamis in the Sea of Japan.

Introduction

Since the 20th century, several large (M ~ 7 or larger) earthquakes have occurred in the Sea of Japan (Fig. 1) that caused damage due to seismic ground motion and tsunamis on the coast (Earthquake Research Committee (ERC) 1999). These earthquakes were analyzed using seismic and tsunami data to estimate the source region and fault parameters.

Off Hokkaido, the 1940 off Shakotan Peninsula earthquake (M_{JMA} 7.5) (also called Shakotan-hanto-oki, off the Cape of Kamui, or off the coast of Kamui) occurred and caused a tsunami. There was little damage from the seismic ground motion, but the coastal tsunami height was greater than 2 m at Teshio and Haboro in Hokkaido and Nevelsk in Sakhalin, and there were 10 casualties near the estuary of the Teshio River. The coastal tsunami height on Rishiri Island reached 3 m, and there was light damage to Sado Island and North Korea. In addition, 24 people were injured and 20 houses were washed away by the earthquake and tsunami (Hatori 1969; ERC 2003; Usami et al. 2013).

Various studies on the fault parameters of this earthquake have been documented. Hatori (1969) estimated the tsunami source area from the tsunami travel time data and inverse refraction diagram. Fukao and Furumoto (1975) obtained the focal mechanism solution from the P-wave initial motion, estimated the rupture area from the tsunami source area obtained by Hatori (1969), and calculated the slip amount and seismic moment using long-period surface wave and tsunami data. Satake (1986) revisited the tsunami waveforms, compared the observed waveforms with those calculated by tsunami numerical simulation, and reexamined the fault area, concluding that it was decidedly smaller than that determined by Hatori (1969) and Fukao and Furumoto (1975). Okamura et al. (2005) investigated the fault location from the traces of past earthquakes using seafloor diving surveys, and estimated the fault slip by tsunami waveform inversion. Ohsumi and Fujiwara (2017) compiled fault models based on seismic reflection survey data and validated a suitable model to explain coastal tsunami heights along the Hokkaido coast.

The 1993 off the southwest of Hokkaido earthquake (M_{JMA} 7.8), also known as the 1993 Hokkaido Nansei-oki earthquake, caused the most serious damage along the coast of the Sea of Japan during the 20th century. The coastal tsunami heights reached over 20 m on Okushiri Island and 7–8 m on the west coast of the Oshima Peninsula. The source area of this earthquake was close to Okushiri Island and the west coast of the Oshima Peninsula, and the tsunami struck those regions within 2–5 min. In total, this event caused the death or disappearance of 230 people, with 323 injured, and 601 houses completely destroyed (Hokkaido Tsunami Survey Group 1993; ERC 1999; ERC 2003). Previous studies have analyzed factors relating to this earthquake. Hatori (1994) estimated both the tsunami source area from the tsunami travel times using an inverse refraction diagram and the tsunami magnitude. Tanioka et al. (1995) approximated the fault geometry using seismic waveforms, and obtained the slip distribution from the joint inversion of tsunami and geodetic data. Mendoza and Fukuyama (1996) performed seismic waveform inversion using the strong ground motion data in Japan and teleseismic vertical P-waves, and estimated the slip distribution. Kakehi and Irikura (1997) examined the high-frequency radiation process on the fault plane from the envelope inversion of acceleration seismograms. Takahashi et al. (1994, 1995a, 1995b) investigated the fault model based on the observed coastal tsunami heights and ground deformation using tsunami numerical simulation.

The 1983 Central Sea of Japan earthquake (M_{JMA} 7.7) (also called the Japan Sea earthquake, the Nihonkai-Chubu earthquake, the Akita-oki, and others) struck near the Akita and Aomori Prefectures of the Tohoku region and caused tsunami damage. Its largest aftershock (M_{JMA} 7.1) occurred approximately one month after the mainshock. In the coastal plains of the Aomori and Akita Prefectures, liquefaction damaged structures. The coastal tsunami heights of this earthquake reached 14 m near Noshiro in the Akita Prefecture, 4.3 m on Okushiri Island in Hokkaido, and up to 3 m on the coast of the Chugoku region. As early as 7 min after the earthquake, the tsunami struck the coast near the source area. The damage included 104 casualties (100 caused by the tsunami) with 163 injured, 934 houses completely destroyed, and 52 washed away. The tsunami also caused damage in Korea and Russia (Shuto 1983; ERC 1999; Usami et al. 2013). Hatori (1983) estimated the tsunami source area and the tsunami magnitude. Aida

(1984) compared the observed tsunami waveforms with those calculated by tsunami numerical simulation for many fault models and adopted the model that fit the aftershock distribution. Kanamori and Astiz (1985) conducted moment tensor inversion using long-period surface waves and estimated the slip amount on the fault plane, which was inferred from the aftershock distribution. Sato (1985) examined the high-frequency characteristics of the strong motion records and proposed a three-stage rupture process on the fault planes that were estimated from the aftershock distribution. Satake (1985) estimated the focal mechanism solution and fault plane from long-period surface waves, P-wave initial motion, and aftershock distribution, and determined the fault model by a trial and error comparison of the observed tsunami waveforms with those from numerical simulations. Kosuga et al. (1986) assumed the fault plane based on the aftershock distribution and the models of Sato (1985), and then chose the best fault model to explain the tsunami waveform and crustal deformation among certain models with different slip amounts. Fukuyama and Irikura (1986) examined the rupture process using seismic waveform inversion based on the Bayesian approach, which assumed the moment release and rupture start time as unknown parameters. Satake (1989) improved the fault model of Satake (1985) and estimated the slip amount by tsunami waveform inversion using Japanese tide gauge records. For the largest aftershock (M_{JMA} 7.1), Hatori (1984) estimated the tsunami source area and tsunami magnitude. Abe (1987) also estimated the tsunami source area and examined the fault model by conducting tsunami numerical experiments to compare the observed waveforms and travel times with the calculated data.

The 1964 off Oga Peninsula earthquake (M_{JMA} 6.9) occurred near the Akita Prefecture, but its damage along the coast of the Tohoku region was minimal. Small tsunami amplitudes (~ 20 cm) were recorded at the tide gauge stations along the coast of Hokkaido to the Niigata Prefecture (Hatori 1965; ERC 2003; Usami et al. 2013). Hatori (1965) estimated the tsunami source area for this earthquake. Fukao and Furumoto (1975) estimated the seismic moment by comparing the amplitudes of the long-period Love waves from the World-Wide Standardized Seismograph Network (WWSSN) to the synthetic data, and then calculated the slip amount on the fault plane, which was estimated from the aftershock distribution.

Along the eastern margin of the Sea of Japan, many offshore active faults have been investigated, many of which are summarized by Okamura (2019). A government committee jointly supported by the Ministry of Land, Infrastructure, Transport and Tourism (MLIT), the Ministry of Education, Culture, Sports, Science and Technology, and the Cabinet Office of Japan, modeled 60 offshore active faults in the Sea of Japan with the potential to cause large earthquakes, and created a tsunami simulation for each (MLIT, 2014). More recently, the Integrated Research Project on Seismic and Tsunami Hazards around the Sea of Japan (hereafter referred to as the JSPJ: Japan Sea Project) modeled the active faults along the Sea of Japan in detail (JSPJ, 2021) (Fig. 2).

In this study, we examined which active faults that have been modeled by the JSPJ may have caused the 20th century earthquakes. For the 1964 off Oga Peninsula and the 1983 west off Aomori earthquakes, no fault models have been obtained from previous studies. Therefore, we relocated the hypocenters and estimated the fault plane geometries using seismic data, developed teleseismic waveform inversions to obtain the slip distributions, and estimated the fault models. For the above five earthquakes, we

conducted tsunami simulations using previous studies or the teleseismic waveform inversion of this study, as well as nearby fault models obtained from the JSPJ, and attempted to identify the causative fault by comparing the calculated tsunami waveforms and the coastal tsunami heights with the observed data.

Seismic Analysis For The 1964 Oga And The 1983 West Off Aomori earthquakes

Relocation and determination of focal mechanism

For the two M ~ 7 earthquakes, we relocated the hypocenters, determined the focal mechanism for each mainshock, and estimated the fault plane geometry by hypocenter relocation of the mainshock and aftershocks.

For the mainshock relocation, the arrival times and time differences of P, S, pP, and sP waves at worldwide stations from the ISC catalog were used with the location software HYPOSAT (Schweitzer 2001). Theoretical travel times were calculated using the seismic velocity structure ak135 (Kennett et al. 1995), and crustal heterogeneity was considered by adopting the CRUST2.0 model (Bassin et al. 2000). The dip angle of the fault plane was estimated from the accurate relative hypocenter locations of the mainshock and aftershocks (within 3 days of the mainshock), which were relocated by the Modified Joint Hypocenter Determination (MJHD) method (Hurukawa 1995).

Teleseismic waveform inversion

We performed the teleseismic waveform inversion (Kikuchi and Kanamori 1991; Kikuchi et al. 1993) to obtain the slip distribution for each earthquake using the relocated hypocenter and the estimated fault plane. The non-negative least square method with smoothing in both space and time for slip distribution were applied to the inversion as the constraint conditions. P-wave vertical components were obtained from the World Wide Standardized Seismograph Network (WWSSN) records. The synthetic waveforms were calculated using the velocity structure of ak135 (Kennett et al. 1995), and crustal heterogeneity was considered by adopting the CRUST2.0 model (Bassin et al. 2000).

Tsunami analysis

Observed tsunami data

In addition to the tsunami records of Japan and Korea, which have been used in previous studies (Satake 1989; Tanioka et al. 1995; Okamura et al. 2005), those of the Sakhalin and Primorye regions in Russia was also employed (Fig. 3). The coastal tsunami runup heights were obtained from the Japan Tsunami Trace database of the International Research Institute of Disaster Science, Tohoku University.

Estimation of seafloor displacements

For the offshore active faults mapped by JSPJ (2021), the slip amounts of possible earthquakes were estimated from the two types of scaling relations. The first is the relationship between seismic moment and source area that was developed by the ERC under the Headquarters for Earthquake Research Promotion to predict strong ground motions for inland active faults with known geometry (ERC 2020; hereafter we refer to it as "Recipe"). The second is the association between seismic moment and fault length as indicated by Takemura (1998), which was obtained from inland earthquake data in Japan. We then calculated the slip amount as $M_0 = \mu \times D \times S$, where μ, D, and S are the rigidity, slip amount, and source area, respectively. In the “Recipe,” different relations are based on three stages: Somerville et al. (1999) for $M_w \leqq 6.5$ earthquakes, Irikura and Miyake (2001) for $6.5 < M_w \leqq 7.4$, and Murotani et al. (2015) for $M_w > 7.4$. The details of the scaling relations and the estimation of the slip amount are described by Satake et al. (in this special issue). The seafloor displacement was calculated by the formulas of Okada (1985) using the fault parameters including the slip amount.

Tsunami numerical simulation

For the tsunami numerical simulation, we created a 9-arcsec (approximately 270 m in latitude direction) interval bathymetry grid from JTOPO30 and M7000 series digital bathymetry data provided by the Marine Information Research Center for the Japanese coasts, and GEBCO2020 (GEBCO Compilation Group 2020) for the Korean and Russian coasts. The nonlinear long-wave equations of the program code of JAGURS (Baba et al. 2015) were solved, and the waveforms for 3 h after each earthquake were calculated.

The 1940 Off Shakotan Peninsula Earthquake

The fault models used for the tsunami numerical simulation of the 1940 off Shakotan Peninsula earthquake were: MS01, MS02, ST01, and ST02 of the JSPJ (Fig. 2), the Okamura et al. (2005) model, and the HKD-2239 model of Ohsumi and Fujiwara (2017). The multiple fault model MS01 + MS02 + ST01 + ST02 (referred to as Model A) corresponds to the location of the fault model in previous studies (Okamura et al. 2005; Ohsumi and Fujiwara 2017). The slip amounts calculated by the "Recipe" and Takemura (1998) are referred to as Model Ar and Model At, respectively (hereafter, the same naming applies to other earthquakes). Table 1 lists the fault parameters for each fault model. The top depths of all the faults were assumed to be the seafloor. Figure 4 shows the seafloor displacements that were used as the initial conditions of the tsunami numerical simulation for each model. Tide gauge records at Ishikari, Otaru, Oshoro, Iwanai, Sakata, Niigata, Wajima, Nevelsk, Bolshoy Kamen, and Vladivostok were used for comparison with simulated tsunami waveforms. In addition to the Japanese records used by Okamura et al. (2005), we added Nevelsk in Sakhalin and Bolshoy Kamen and Vladivostok in Primorye to the north and the southwest of the source area, respectively.

We compared the observed tsunami waveforms with the calculated ones for each model (Fig. 5). For the Russian records, the accuracies of clock timing and bathymetry data around the stations were unknown; therefore, the first motions of the observed waveforms were aligned with those of their calculated waveforms. In the case of Model At, the calculated waveforms were substantially larger in amplitude than those observed. Therefore, Model At was plotted at half the amplitude, as shown in Fig. 5. Model Ar closely reproduced the observed waveform at Nevelsk to the north of the source area, but the first motions of the calculated waveforms were opposite to those observed at Ishikari, Otaru, Oshoro, and Iwanai to the southeast of the source area. The fault models of Okamura et al. (2005) and Ohsumi and Fujiwara (2017) were comparable to the waveforms of the Japanese observations, but did not reproduce the first wave observed at Nevelsk.

To differentiate Model Ar and Okamura et al. (2005), we calculated the contribution from each subfault to the calculated waveforms (Fig. 6). Regarding Model Ar, the calculated first wave at Nevelsk was caused by the northernmost fault MS01 (slip is 3.28 m), and the calculated first downward motion at Ishikari, Iwanai, and Oshoro was related to the slip of the southern fault ST01 (2.43 m). In contrast, the small amplitude of Nevelsk calculated by the model of Okamura et al. (2005) was due to the small slip (1.6 m) of the northernmost Kita Oshoro seamount. The calculated first waves at the tide gauge stations in Hokkaido were the result of a large slip (2.7 m) at the Minami Oshoro seamount and a small slip (0.6 m) at the Kaiyo seamount.

We further compared the observed and calculated tsunami heights along the Japanese coasts (Fig. 7). The coastal tsunami trace heights for this earthquake were identified at 22 points in the Hokkaido region and four in Chubu to Kinki regions, with the farthest point from the source located at Kyotango City, Kyoto Prefecture. Here, the K value (geometric mean of the observed coastal tsunami heights to the calculated values) proposed by Aida (1977) was used as an index of the comparison (Table 1). From the K value and Fig. 7, the calculated coastal tsunami heights of Model At were identifiably larger than the observations, similar to the tsunami waveforms. The K value of Model Ar was the superior ($K = 1.01$) among the four models. From the comparison of the tsunami waveforms and the coastal tsunami heights, it appears that the four faults in Model A (MS01, MS02, ST01, and ST02) caused this earthquake, but the slip amount of the ST01 fault requires further examination.

Table 1
List of fault parameters for the 1940 off Shakotan Peninsula earthquake (M_{JMA} 7.5)

Model	Fault	M_w	Length (km)	Width (km)	Strike (°)	Dip (°)	Rake (°)	Slip (m)	K
Model Ar	MS01	7.8	57.1	32.0	9	30	53	3.28	1.01
	MS02		40.3	22.6	183	45	82	2.32	
	ST02		59.6	28.0	357	30	45	3.13	
	ST01		40.4	24.9	171	40	94	2.43	
Model At	MS01	8.1	57.1	32.0	9	30	53	8.79	0.38
	MS02		40.3	22.6	183	45	82	8.78	
	ST02		59.6	28.0	357	30	45	10.48	
	ST01		40.4	24.9	171	40	94	8.00	
Okamura et al. (2005)	Kita Oshoro	7.5	42.0	16.0	22	45	90	1.64	1.59
	Oshoro		42.0	16.0	184	45	90	2.23	
	Minami Oshoro		37.0	16.0	162	45	90	2.74	
	Kaiyo		53.0	16.0	0	45	90	0.58	
Ohsumi and Fujiwara (2017): HKD-2239	HKD-39	7.4	33.9	16.9	189	45	90	3.0	1.29
	HKD-38		15.1	16.9	162	45	90	3.0	
	HJD-22		30.3	16.9	189	45	90	3.0	
			28.9	16.9	167	45	90	3.0	

The 1993 Off The Southwest Coast Of Hokkaido Earthquake

The fault models used for the tsunami numerical simulation of the 1993 off the southwest coast of Hokkaido earthquake were: OK03a, OK03b, and OK05 of the JSPJ (Fig. 2), along with the models of Tanioka et al. (1995) and Takahashi et al. (1995a). The multiple fault model OK03a + OK03b + OK05 (referred to as Model A) is located close to the models in previous studies (Tanioka et al. 1995; Takahashi et al. 1995a), although their northernmost faults do not correspond to any of the JSPJ fauls. In addition, the northernmost faults of Tanioka et al. (1995) and Takahashi et al. (1995a) have different dip directions, east and west dipping, respectively. Table 2 lists the fault parameters for each fault model, and Fig. 8 shows the seafloor displacements calculated from the models.

The tide gauge records at Wakkanai, Kutsugata, Rumoi, Iwanai, Otaru, Esashi, Yoshioka, Ohminato, Nezugaseki, Awashima, Iwafune, Teradomari, Kashiwazaki, Toyama, Fushiki, Fukui, Sokcho, Mukho,

Uglegorsk, Nakhodoka, Vladivostok, and Posyet were compared with the simulated tsunami waveforms (Fig. 3). In addition to the Japanese and Korean records used in Tanioka et al. (1995), those of Uglegorsk in Sakhalin, and Nakhodoka, Vladivostok, and Posyet in Primorye were added for the north and west regions of the source area, respectively.

Figure 9 shows a comparison between the observed and calculated tsunami waveforms for each model. For the Russian records, the first motions of the observed waveforms were aligned with those of the calculated waveforms. In the case of Model At and the Takahashi et al. (1995a) model, the calculated waveforms were larger in amplitude compared with the observed waveforms at most of the tide gauge stations. Therefore, these models were plotted at half of the amplitude (Fig. 9). The phases of the waveforms of Model Ar and Tanioka et al. (1995) were similar, and closely matched the observed waveforms except for the short-period components, but the amplitude of the waveforms calculated by Tanioka et al. (1995) were closer to the observed waveforms than those of Model Ar.

We compared the observed and calculated tsunami heights for this earthquake (Fig. 10 and Table 2) along the Japanese coast. The coastal tsunami trace heights were measured in a considerably wide area, with 209 points in Hokkaido and 110 points in Honshu, extending from the Tohoku to Chugoku regions. The farthest point from the source was Hamada City, Shimane Prefecture. On the southern coast of Okushiri Island near the source area, tsunami trace heights were found to be over 20 m. The model with the best K value (Aida 1977) was that of Takahashi et al. (1995a) (K = 1.03), which fit the observed coastal tsunami heights. Model At (K = 1.09) explained the observed coastal tsunami heights well, but the maximum peak of the calculation appeared slightly north of the observations. However, none of the models could relate the large tsunami heights of over 20 m on southern Okushiri Island.

JSPJ faults ST06, ST07, ST08, ST09, OK01, and OK02 also exist in this region (Fig. 2). Therefore, we examined the combinations of these faults, but they were not able to reproduce the observed waveforms (see Additional file 1: Fig.S1–S2). In addition, there are too few coastal tsunami trace heights observed to the north of the source area (Fig. 10) to select appropriate fault models using the K values (Aida 1977).

From the above examinations, Model Ar and Model At reproduced the tsunami waveforms and the coastal tsunami heights, respectively. From the comparison of the tsunami waveforms and the coastal tsunami heights, the three faults in Model A (OK03a, OK03b, and OK05) appear to be responsible for this earthquake. The reason for the inability of the models to reproduce the large tsunami runup heights of greater than 20 m may be due to the coarse grid size of the tsunami numerical simulation (9-arcsec), which does not reproduce the detailed local topography.

Table 2
List of fault parameters for the 1993 off the southwest coast of Hokkaido earthquake (M_{JMA} 7.8)

Model	Fault	M_w	Length (km)	Width (km)	Depth (km)	Strike (°)	Dip (°)	Rake (°)	Slip (m)	K
Model Ar	OK03a	7.5	27.6	19.8	0.0	176	45	100	2.29	2.26
	OK03b		20.4	19.8	0.0	210	45	112	1.97	
	OK05		59.6	21.2	0.0	171	45	95	3.49	
Model At	OK03a	7.7	27.6	19.8	0.0	176	45	100	4.35	1.09
	OK03b		20.4	19.8	0.0	210	45	112	3.21	
	OK05		59.6	21.2	0.0	171	45	95	8.75	
Tanioka et al. (1995)		7.8	27.0	40.0	0.0	340	30	90	2.16	1.52
			25.0	30.0	0.0	200	30	90	0.52	
			25.0	30.0	0.0	200	30	90	6.07	
			27.0	30.0	0.0	160	60	90	3.10	
			35.0	30.0	0.0	260	60	90	3.79	
Takahashi et al. (1995a)		7.8	90.0	25.0	10.0	188	35	80	5.71	1.03
			26.0	25.0	5.0	175	60	105	4.0	
			30.5	15.0	5.0	150	60	105	12.0	

The 1983 West Off Aomori Earthquake

The 1983 west off Aomori earthquake was the largest aftershock of the 1983 Central Sea of Japan earthquake (M_{JMA} 7.7). We relocated the hypocenter of the earthquake and determined the fault mechanism solution (Fig. 11). The hypocenter relocated using HYPOSAT with 542 onset times at 487 stations and five travel-time differences at five stations was at 41.37° N, 139.08° E, and a depth of 20 km (orange star in Fig. 11). The focal mechanism from the Global CMT solution is a reverse fault with strike, dip, and rake of 198°, 47°, and 87° and 23°, 43°, and 94°, respectively (beach ball in Fig. 11). Based on the relative hypocenter locations of this earthquake and its aftershocks relocated by the MJHD method (Hurukawa 1995) using the data from 101 stations (Fig. 11), we assumed that the fault plane of this earthquake was the east-southeast dipping plane with a strike of 23° and a dip of 43° (AB section in Fig. 11).

Using the relocated epicenter and the east-southeast dipping fault plane of this earthquake, we performed a teleseismic waveform inversion using the vertical component of P-waves at 14 stations (Fig. 12a) to estimate the fault parameters. The depth of the hypocenter obtained using HYPOSAT was 20 km, but we

finally set it at 12 km by trial and error in the inversion process. The final parameters obtained were as follows: the fault mechanism (strike, dip, rake) was 23°, 43°, and 85°, respectively (Fig. 12b); the source time was approximately 20 s (Fig. 12b); the maximum slip was 2.24 m; the average slip was 0.45 m (Fig. 12c); and the seismic moment was 3.1×10^{19} Nm (M_w 6.9). The observed and synthetic waveforms were in good agreement (Fig. 12d).

The fault models used for the tsunami numerical simulation of the 1983 west off Aomori earthquake are the MMS02 of the JSPJ (Model A), the seismic inversion model (Fig. 12c), and the uniform slip model, which was modified from the seismic inversion model. Table 3 lists the fault parameters for each model. The top depths of all the faults were assumed to be the seafloor. Figure 13 shows the seafloor displacements calculated from each model. The tide gauge stations using the tsunami numerical simulation were at Wakkanai, Senboshi, Ishikari, Iwanai, Esashi, Yoshioka, Fukaura, Noshiro, Funakawa, Awashima, Iwafune, Ryotsu, and Naoetsu (Fig. 3).

Figure 14 compares the observed and the calculated tsunami waveforms for each model. The amplitudes of calculated waveforms from Model At were larger than the observed ones, and those from the seismic inversion model were slightly smaller than those observed. The amplitudes calculated by Model Ar and the uniform slip model were larger than those of the seismic inversion model, and more similar to those observed. The dip directions of Model A and the seismic inversion model were the west and east dipping, respectively. As a result, the tsunami first motion at Fukaura and the waveforms around the first and second phases at Fukaura and Noshiro were slightly different, and the seismic inversion model produced tsunami waveforms closer to those observed than Model A.

The fault plane estimated from the aftershock distribution was east dipping, but the MMS02 obtained from the offshore active fault survey was west dipping. The 1983 Central Sea of Japan earthquake, which was the mainshock of this earthquake, had an east dipping fault plane; therefore, the aftershock distribution (Fig. 11) may be influenced by the mainshock, although there are no results strongly indicating that this earthquake occurred on MMS02.

Table 3
List of fault parameters for the 1983 west off Aomori earthquake (M_{JMA} 7.1)

Model	Fault	M_w	Length (km)	Width (km)	Strike (°)	Dip (°)	Rake (°)	Slip (m)
Model Ar	MMS02	6.9	40.6	18.2	220	40	130	1.20
Model At	MMS02	7.2	40.6	18.2	220	40	130	2.84
Seismic inversion model		6.9	50.0	30.0	23	43	85	ave. 0.45
Uniform slip model		7.0	50.0	30.0	23	43	85	0.73

The 1983 Central Sea Of Japan Earthquake

The fault models used for the tsunami numerical simulation of the 1983 Central Sea of Japan earthquake were: MMS01, MMS02, MMS03, MMS04, and MGM01 of the JSPJ, and that of Satake (1989). The multiple fault model MMS01 + MMS04 + MGM01 (referred to as Model A) corresponded to the location of the Satake (1989) model, and we set the model with MMS02 and MMS03 as Model B (MMS01 + MMS04 + MGM01 + MMS02 + MMS03). For Model B, since MMS02 and MMS03 cross MMS01, we did not consider the slip amount using Takemura (1998), which depends on the total length of subfaults, and instead used only those calculated by the "Recipe" (Model Br). Table 4 and Fig. 15 show the fault parameters and calculated seafloor displacements for each model.

The tide gauge records at Kutsugata, Ishikari, Iwanai, Esashi, Yoshioka, Sakata, Kashiwazaki, Toyama, Rudnaya Pristan, Nakhodoka, Vladivostok, and Posyet were compared with simulated tsunami waveforms. In addition to the Japanese records used in Satake (1989), Rudnaya Pristan, Nakhodoka, Vladivostok, and Posyet in Primorye were added to cover the northwest direction of the source area.

Figure 16 shows a comparison between the observed and calculated tsunami waveforms for each model. For the Russian records, the first motions of the observed waveforms were aligned with those of the calculated waveforms. In the case of Model At and Model Br, the calculated waveforms were larger in amplitude than the observed waveforms at Yoshioka near the source area, and their models were plotted at half of the amplitude (Fig. 16). Regarding MMS01 of the JSPJ, the slip amount of Model Br (3.37 m) is similar to that of Model Ar (3.09 m) (Table 4), but the amplitude of the tsunami waveforms of Model Br was closer to the amplitude of Model At (with a slip amount of 5.54 m) because Model Br included contributions from MMS02 and MMS03. These additional faults caused the larger amplitudes of the tsunami waveforms over the observations. The calculated first motion of Model A at Esashi showed a slight downward trend, while that from Model Br (with MMS02 + MMS03 to Model A) was upward and consistent with the observed waveform. At the other stations, there was little difference in the phases of the calculated tsunami waveform among the fault models.

We compared the observed and calculated tsunami heights (Fig. 17 and Table 4) along the Japanese coast. For this earthquake, the coastal tsunami trace heights were measured in a wide area, with 133 points in Hokkaido and 613 points in Honshu, extending from the Tohoku to Kyushu regions. The farthest point from the source was Tsushima City, Nagasaki Prefecture. The model with the best K value (Aida 1977) was Model At (K = 1.22); however, the maximum peak of the calculated coastal tsunami height was to the north of the coastal tsunami trace heights because the northernmost fault MMS01 had the largest slip amount (5.44 m). None of the models could explain the tsunami heights greater than 10 m along the coast near Noshiro.

Based on the comparison of the tsunami waveform amplitudes and the coastal tsunami heights, the JSPJ fault Model A may have caused this earthquake; Model A is near the location of Satake (1985, 1989), which was obtained based on the aftershock distribution.

Table 4
List of fault parameters for the 1983 Central Sea of Japan earthquake (M_{JMA} 7.7)

Model	Fault	Mw	Length (km)	Width (km)	Depth (km)	Strike (°)	Dip (°)	Rake (°)	Slip (m)	*K*
Model Ar	MMS01	7.7	53.2	33.4	0.0	334.0	25.0	69.0	3.09	1.95
	MMS04		21.8	33.1	0.0	21.0	25.0	89.0	1.98	
	MGM01		53.2	33.8	0.0	26.0	25.0	69.0	3.12	
Model At	MMS01	7.8	53.2	33.4	0.0	334.0	25.0	69.0	5.44	1.22
	MMS04		21.8	33.1	0.0	21.0	25.0	89.0	2.25	
	MGM01		53.2	33.8	0.0	26.0	25.0	69.0	5.36	
Model Br	MMS01	7.8	53.2	33.4	0.0	334.0	25.0	69.0	3.37	1.72
	MMS04		21.8	33.1	0.0	21.0	25.0	89.0	2.15	
	MGM01		53.2	33.8	0.0	26.0	25.0	69.0	3.39	
	MMS02		40.6	18.2	0.0	220.0	40.0	130.0	2.18	
	MMS03		29.7	18.0	0.0	205.0	45.0	108.0	1.85	
Satake (1989)		7.7	30.0	40.0	1.0	340.0	30.0	90.0	1.80	1.98
			30.0	40.0	1.0	340.0	30.0	90.0	2.20	
			30.0	40.0	1.0	20.0	30.0	90.0	3.90	
			30.0	40.0	1.0	20.0	30.0	90.0	2.00	

The 1964 Off Oga Peninsula Earthquake

We relocated the hypocenter of the 1964 off Oga Peninsula earthquake and determined the fault mechanism solution (Fig. 18). The hypocenter relocated using HYPOSAT with 331 onset times at 270 stations and 19 travel-time differences at 15 stations was at 40.42° N, 139.00° E, and a depth of 20.8 km (orange star in Fig. 18). The focal mechanism obtained using teleseismic P-waves at 39 stations was a reverse fault with a strike, dip, and rake of 238°, 43°, and 117° and 24°, 53°, and 68°, respectively (beach ball in Fig. 18). Based on the relative hypocenter locations of this earthquake and its aftershocks relocated by the MJHD method (Hurukawa 1995) using the data from 79 stations, we assumed that the fault plane of this earthquake was the south-southeast dipping plane with a strike of 24° and a dip of 53° (AB section in Fig. 18).

Using the relocated hypocenter and the south-southeast dipping fault plane of this earthquake, we performed a teleseismic waveform inversion using the vertical component of P-waves at 23 stations (Fig. 19a) to estimate the fault parameters. The obtained final parameters were as follows: the fault

mechanism (strike, dip, rake) was 24°, 53°, and 71°, respectively (Fig. 19b); the source time was approximately 20 s (Fig. 19b); the maximum slip was 1.36 m; the average slip was 0.16 m (Fig. 19c); and the seismic moment was 1.5×10^{19} Nm (M_w 6.8). The observed and synthetic waveforms were in good agreement (Fig. 19d).

The fault models used for the tsunami numerical simulation of this earthquake were MGM02 (referred to as Model A), MGM03 (Model B), MMS06 (Model C) of the JSPJ, the teleseismic inversion model, and the uniform slip model, which was modified from the teleseismic inversion model. The aftershock distribution suggests a south-southeast dipping fault plane, while the surrounding JSPJ offshore active faults show northwest dipping fault planes. Table 5 and Fig. 20 show the fault parameters and calculated seafloor displacements for each model. The top depths of all the faults were assumed to be the seafloor. The tide gauge stations using the tsunami numerical simulation were Esashi, Fukushima, Iwasaki, Funakoshi, Funakawa, Akita, Shimotsu, and Niigata. There have been no documented studies examining the fault parameters using these tsunami waveforms.

Figure 21 shows comparisons between the observed and the calculated tsunami waveforms for each model. The amplitudes of tsunami waveforms calculated from the teleseismic inversion model were slightly smaller than the observed waveforms, but those from the uniform slip model were more similar to the observations. The amplitude of tsunami waveforms calculated from Model At was larger than Model Ar, and substantially larger than the observed tsunami waveform at Iwasaki near the source area. Model B displayed similar features to Model A. The amplitudes of the calculated tsunami waveforms of Model Cr and Model Ct were comparable because the slip amounts were approximately equal, but there were some stations whose amplitudes were twice as large as the observed tsunami waveforms (Fig. 21). The calculated tsunami waveforms of Model A, Model B, and the seismic inversion model were similar even at stations near the source area. Therefore, it is difficult to determine which fault and which fault dip direction caused this earthquake.

Table 5
List of fault parameters for the 1964 off Oga Peninsula earthquake (M_{JMA} 6.9)

Model	Fault	M_w	Length (km)	Width (km)	Strike (°)	Dip (°)	Rake (°)	Slip (m)
Model Ar	MGM02	6.6	25.2	18.3	209	50	101	0.75
Model At	MGM02	6.9	25.2	18.3	209	50	101	1.75
Model Br	MGM03	6.7	22.8	22.1	225	40	140	0.82
Model Bt	MGM03	6.8	22.8	22.1	225	40	140	1.31
Model Cr	MMS06	7.2	41.1	28.2	195	30	100	1.88
Model Ct	MMS06	7.2	41.1	28.2	195	30	100	1.86
Seismic inversion model		6.8	50.0	40.0	24	53	71	ave. 0.16
Uniform slip model		6.9	50.0	40.0	24	53	71	0.44

Comparison Of Fault Models And Scaling Relations

We considered the relationship between the seismic moment (M_0) and source area (S) for earthquakes occurring in the Sea of Japan. The M_0 and S for the fault models in this study are shown in Fig. 22, along with the scaling relations used in the "Recipe" (Somervile et al. 1999; Irikura and Miyake 2000; Murotani et al. 2015). The scaling relation of the "Recipe" has three stages at bending points M_w 6.5 and M_w 7.4.

The fault models obtained from the tsunami waveform inversions for the 1940 off Shakotan Peninsula, the 1993 off the southwest coast of Hokkaido, and the 1983 Central Sea of Japan earthquakes are in good agreement with the third stage (solid circle, solid square, and solid triangle in Fig. 22). The fault model of Ohsumi and Fujiwara (2017) for the 1940 off Shakotan Peninsula earthquake estimated from the coastal tsunami trace heights (open circle in Fig. 22) also correlates to the scaling relation. Regarding the 1993 off the southwest coast of Hokkaido earthquake, the model of Takahashi et al. (1995a) estimated from the coastal tsunami trace heights (open square in Fig. 22) is out of the scaling relation because a large slip amount was required to explain the coastal tsunami heights. The Model At for the 1940, 1993, and 1983 earthquakes for which the Takemura (1998) was adopted is also out of the scaling relation and is located on the extension of the second stage of Irikura and Miyake (2001). The calculated tsunami waveforms from Model At are exceptionally large, which supports the requirement for the third stage of the scaling relation.

The relationship between M_0 and S for the 1964 off Oga Peninsula and the 1983 west off Aomori earthquakes are also out of the scaling relation (diamond and inverted triangle in Fig. 22), which were estimated from the teleseismic waveform inversion. Although the fault area assumed in the teleseismic

inversion was large, the slip concentration area was small. Hence, the actual rupture area may be closer to the scaling relation. The slip amount obtained from the teleseismic waveform inversion was too small to accurately reproduce the amplitude of the tsunami waveform, while the models using the slip amount obtained by the “Recipe" more accurately reproduced the amplitude (orange and purple stars in Fig. 22).

Conclusion

For M ~ 7 or larger earthquakes that occurred in the Sea of Japan during the 20th century, we examined which active faults that were modeled by the JSPJ may have been the cause. For large earthquakes with M ≥ 7.5, the mapped offshore active faults and those estimated from seismic and tsunami studies were located in a similar area, and the observed tsunami waveforms were reproduced by applying the slip amount calculated by the scaling relation to the mapped offshore active faults. For the 1940 off Shakotan Peninsula earthquake, MS01, MS02, ST01, and ST02 of the JSPJ which corresponds to the location of the fault model obtained by tsunami studies (Okamura et al. 2005; Ohsumi and Fujiwara 2017) appear to have been responsible. For the 1993 off the southwest coast of Hokkaido earthquake, OK03a, OK03b, and OK05 of the JSPJ which corresponds to the part of the fault model obtained by tsunami studies (Tanioka et al. 1995; Takahashi et al. 1995a) are likely the cause. The 1983 central Sea of Japan earthquake appears to relate to MMS01, MMS04, and MGM01 of the JSPJ, which corresponds to the location of the fault model obtained by tsunami waveform inversion (Satake 1989). In the case of the M ~ 7 earthquakes, the fault locations estimated using seismic data in this study did not match the mapped offshore active faults, and the dip directions differed. For the 1983 west off Aomori earthquake, both the faults of MMS02 and that obtained by the teleseismic waveform inversion could reproduce the observed waveforms given an appropriate slip amount. Therefore, it was not possible to confirm which fault caused the earthquake by comparing the tsunami waveforms. Regarding the 1964 earthquake, it was also not possible to identify the causative fault among MGM02, MGM03, MMS06, and that obtained by teleseismic waveform inversion. Teleseismic waveform inversion for an M ~ 7 earthquake can adequately provide the seismic moment, while the fault location and rupture area cannot be accurately determined. For further evaluation of the two M ~ 7 earthquakes, analysis using near-field waveforms may be necessary.

In this study, a nonlinear long-wave equation was solved in the tsunami numerical simulation. In order to further improve the reproducibility of the observed tsunami waveforms and the coastal tsunami trace heights, more careful analysis may be needed, such as the application of the Kajiura filter (Kajiura 1963), a consideration of dispersion, and high-resolution bathymetry data around the tide gauge stations, as well as topography data near the coastal runup points. The slip amount calculated by the empirical scaling relation does not necessarily agree with that of the model by the tsunami waveform inversion or the model to explain the coastal tsunami trace heights. However, it was confirmed that the observed tsunami waveforms can be reproduced by applying the scaling relation with three stages between the seismic moment and fault area, which was originally developed for inland active faults for large earthquakes in the Sea of Japan. By using the scaling relation, we can obtain the slip amount and

estimate the coastal tsunami heights and inundation area. These data will be useful for disaster prevention and mitigation against future earthquakes and tsunamis in the Sea of Japan.

Abbreviations

ERC: Earthquake Research Committee under the Headquarters for Earthquake Research Promotion, JSPJ: Japan Sea Project whose official name is the Integrated Research Project on Seismic and Tsunami Hazards around the Sea of Japan, MJHD: Modified Joint Hypocenter Determination, MLIT: Ministry of Land, Infrastructure, Transport and Tourism, JMA: Japan Meteorological Agency

Declarations

Ethics approval and consent to participate

Not applicable

Consent for publication

Not applicable

Availability of data and materials

M7000 series and JTOPO30 bathymetric digital data are published by the Japan Hydrographic Association. GEBCO_2020 Grid is available at https://www.gebco.net/data_and_products/gridded_bathymetry_data/gebco_2020/, doi:10.5285/a29c5465-b138-234d-e053-6c86abc040b9. Tsunami height information in Japan is available at Japan tsunami trace database at https://tsunami-db.irides.tohoku.ac.jp/tsunami/. JAGRUS tsunami simulation code is available at https://github.com/jagurs-admin/jagurs.

Competing interests

Not applicable

Funding

The study was supported by the Integrated Research Project on Seismic and Tsunami Hazards Around the Sea of Japan from the Ministry of Education, Culture, Sports, Science and Technology of Japan.

Authors' contributions

SM performed seismic and tsunami analyses for all the earthquakes and drafted the manuscript. KS led the project and contributed to the interpretation of results and writing of the manuscript. TI contributed to the interpretation of results. TH conducted seismic analyses for the 1964 and 1983 M~7 earthquakes. All authors read and approved the final manuscript.

Acknowledgements

We would like to thank all the organizations and individuals who provided data, especially the Russian tide gauge data, and the information used in this study. We used the computer systems of the Earthquake and Volcano Information Center of the Earthquake Research Institute, the University of Tokyo. We used Generic Mapping Tools (Wessel and Smith 1998) to draw the figures.

Author details

Satoko Murotani[1,2], Kenji Satake[2], Takeo Ishibe[3,2], and Tomoya Harada[2]

1 National Museum of Nature and Science, Ibaraki, Japan.

2 Earthquake Research Institute, The University of Tokyo, Tokyo, Japan.

3 Association for the Development of Earthquake Prediction, Tokyo, Japan.

Authors' information

Not applicable

Endnotes

Not applicable

References

1. Abe K (1987) Source model and characteristics of a small tsunami —On the tsunami accompanying the largest aftershock (June 21, 1983) of Japan Sea earthquake—. Zisin 40:349–363. https://doi.org/10.4294/zisin1948.40.3_349
2. Aida I (1977) Simulations of large tsunamis occurring in the past off the coast of the Sanriku District. Bull Earthq Res Inst Univ of Tokyo 52:71–101
3. Aida I (1984) A source model of the tsunami accompanying the 1983 Nihonkai-Chubu earthquake. Bull Earthq Res Inst Univ of Tokyo 59:93–104
4. Baba T, Takahashi N, Kaneda Y, Ando K, Matsuoka D, Kato T (2015) Parallel implementation of dispersive tsunami wave modeling with a nesting algorithm for the 2011 Tohoku tsunami. Pure appl Geophys 172(12):3455–3472. doi:10.1007/s00024-015-1049-2
5. Bassin C, Laske G, Masters G (2000) The current limits of resolution for surface wave tomography in North America. EOS Trans AGU 81:F897
6. Earthquake Research Committee (1999) Seismic activity in Japan. Headquarters for Earthquake Research Promotion. http://www.hp1039.jishin.go.jp/eqchreng/eqchrfrm.htm. Accessed 20 Aug 2021

7. Earthquake Research Committee (2003) Long term evaluation for seismic activity along the eastern margin of the Sea of Japan. Headquarters for Earthquake Research Promotion. https://www.jishin.go.jp/main/chousa/kaikou_pdf/nihonkai.pdf. Accessed 20 Aug 2021 (in Japanese)
8. Earthquake Research Committee (2020) Strong ground motion prediction method for earthquakes with specified source faults (“Recipe”) (as of 2020 March 6th). Headquarters for Earthquake Research Promotion. https://www.jishin.go.jp/evaluation/strong_motion/strong_motion_recipe. Accessed 20 Aug 2021 (in Japanese)
9. Fukao Y, Furumoto M (1975) Mechanism of large earthquakes along the eastern margin of the Japan Sea. Tectonophysics 26:247–266. https://doi.org/10.1016/0040-1951(75)90093-1
10. Fukuyama E, Irikura K (1986) Rupture process of the 1983 Japan Sea (Akita-oki) earthquake using a waveform inversion method. Bull Seismol Soc Am 76:1623–1640. https://doi.org/10.1785/BSSA0760061623
11. GEBCO Compilation Group (2020) GEBCO 2020 Grid. https://www.gebco.net/data_and_products/gridded_bathymetry_data/gebco_2020/, doi:10.5285/a29c5465-b138-234d-e053-6c86abc040b9. doi:10.5285/a29c5465-b138-234d-e053-6c86abc040b9. Accessed 20 Aug 2021
12. Hatori T (1965) On the Tsunami which accompanied the Earthquake off the Northwest of Oga on May 7, 1964. Bull Earthq Res Inst Univ of Tokyo 43:149–159
13. Hatori T (1969) A study of the wave source tsunami generated off west Hokkaido on Aug. 2, 1940. Bull Earthq Res Inst Univ of Tokyo 47:1063–1072
14. Hatori T (1983) Tsunami magnitude and source area of the Nihonkai-Chubu (the Japan Sea) earthquake in 1983. Bull Earthq Res Inst Univ of Tokyo 58:723–734 (in Japanese with English abstract)
15. Hatoroi T (1984) The tsunami associated with an aftershock of the 1983 Nihonkai-Chubu earthquake, and the source mechanism of the main tsunami. Bull Earthq Res Inst Univ of Tokyo 59:105–113 (in Japanese with English abstract)
16. Hatori T (1994) Tsunami magnitude and source area of the Southwest off Hokkaido earthquake in 1993. Zisin 47:1–9. https://doi.org/10.4294/zisin1948.47.1_1 (in Japanese with English abstract)
17. Hokkaido Tsunami Survey Group (1993) Tsunami devastates Japanese coastal region. EOS Trans AGU 74:417–432
18. Hurukawa N (1995) Quick aftershock relocation of the 1994 Shikotan Earthquake and its fault planes. Geophys Res Lett 22(23):3159–3162. https://doi.org/10.1029/95GL03167
19. Integrated Research Project on Seismic and Tsunami Hazards around the Sea of Japan (2021) Reports by the Integrated Research Project on Seismic and Tsunami Hazards around the Sea of Japan. https://www.eri.u-tokyo.ac.jp/project/Japan_Sea/houkokusyo.html. Accessed 20 Aug 2021
20. Irikura K, Miyake H (2001) Prediction of strong ground motions for scenario earthquakes. J Geography 110(6):849–875 (in Japanese with English abstract)

21. Kakehi R, Irikura K (1997) High-frequency radiation process during earthquake faulting—envelope inversion of acceleration seismograms from the 1993 Hokkaido-Nansei-Oki, Japan, earthquake. Bull Seismol Soc Am 87(4):904–917
22. Kajiura K (1963) The leading wave of a tsunami. Bull Earthq Res Inst Univ of Tokyo 41:535–571
23. Kanamori H, Astiz (1985) The 1983 Akita-Oki earthquake (Mw = 7.8) and its implications for systematics of subduction earthquakes. Earthq Pred Res 3:305–317. doi:10.1007/978-94-017-2738-9_6
24. Kennett BLN, Engdahl ER, Buland R (1995) Constraints on seismic velocities in the Earth from traveltimes. Geophys J Int 122:108–124. https://doi.org/10.1111/j.1365-246X.1995.tb03540.x
25. Kikuchi M, Kanamori H (1991) Inversion of complex body waves – III. Bull Seismol Soc Am 81(6):2335–2350
26. Kikuchi M, Kananori H, Satake K (1993) Source complexity of the 1988 Armenian earthquake: Evidence for a slow after-slip event. J Geophys Res Solid Earth 98(B9):15797–15808. https://doi.org/10.1029/93JB01568
27. Kosuga M, Ikeda H, Kamazuka Y, Sato H (1986) Static fault model of the 1983 Nihonkai-Chubu (Japan Sea) earthquake as inferred from aftershock distributions, crustal deformation, and tsunami data. J Geod Soc Japan 32(4):290–302 (in Japanese with English abstract)
28. Mendoza C, Fukuyama E (1996) The July 12, 1993, Hokkaido-Nansei-oki, Japan, earthquake: Coseismic slip pattern from strong-motion and telesismic recordings. J Geophys Res Solid Earth 101(B1):791–801. https://doi.org/10.1029/95JB02805
29. Ministry of Land, Infrastructure, Transport and Tourism (2014) Investigation for large earthquakes occurring in the Sea of Japan. Ministry of Land, Infrastructure, Transport and Tourism. http://www.mlit.go.jp/river/shinngikaiblog/daikibojishinchousa. Accessed 20 Aug 2021
30. Murotani S, Matsushima S, Azuma T, Irikura K, Kitagawa S (2015) Scaling relations of source parameters of earthquakes occurring on inland crustal mega-fault systems. Pure Appl Geophys 172(5):1371–1381. https://doi.org/10.1007/s00024-014-1010-9
31. Ohsumi T, Fujiwara H (2017) Investigation of offshore fault modeling for a source region related to the Shakotan-Oki Earthquake. J Disaster Res 12(5):891–898
32. Okada Y (1985) Surface deformation due to shear and tensile faults in a half-space. Bull Seismol Soc Am 75(4):1135–1154. https://doi.org/10.1785/BSSA0750041135
33. Okamura Y (2019) Distribution of active faults in Japan Sea and future issues. Zisin 71:185–199. doi:10.4294/zisin.2017-21 (in Japanese with English abstract)
34. Okamura Y, Satake K, Ikehara K, Takeuchi A, Arai K (2005) Paleoseismology of deep-sea faults based on marine surveys of northern Okushiri ridge in the Japan Sea. J Geophys Res Solid Earth 110:B09105. doi:10.1029/2004JB003135
35. Satake K (1985) The mechanism of the 1983 Japan Sea earthquake as inferred from long-period. surface waves tsunamis Phys Earth Planet Inter 37(4):249–260. https://doi.org/10.1016/0031-9201(85)90012-3

36. Satake K (1986) Re-examination of the 1940 Shakotan-oki earthquake and the fault parameters of the earthquakes along the eastern margin of the Japan Sea. Phys Earth Planet Inter 43(2):137–147. https://doi.org/10.1016/0031-9201(86)90081-6
37. Satake K (1989) Inversion of tsunami waveforms for the estimation of heterogeneous fault motion of large submarine earthquakes: the 1968 Tokachi-oki and 1983 Japan Sea earthquakes. J Geophys Res 94(B5):5627–5636. doi:10.1029/JB094iB05p05627
38. Satake K, Ishibe T, Murotani S, Mulia IE, Gusman AR (2021) Effects of uncertainty in fault parameters on deterministic tsunami hazard assessment: examples for active faults along the eastern margin of the Sea of Japan. Earth Planets Space (this special issue)
39. Sato T (1985) Rupture characteristic of the 1983 Nihonkai-Chubu (Japan Sea) earthquake as inferred from strong motion accelerograms. J Phys Earth 33:525–557. https://doi.org/10.4294/jpe1952.33.525
40. Schweitzer J (2001) HYPOSAT — An enhanced routine to locate seismic events. Pure Appl Geophys 158:277–289. https://doi.org/10.1007/PL00001160
41. Shuto N (1983) Tsunami caused by the Japan Sea earthquake of 1983. Disaster 7(4):255–258
42. Somerville PG, Irikura K, Graves R, Sawada S, Wald D, Abrahamson N, Iwasaki Y, Kagawa T, Smith N, Kowada A (1999) Characterizing crustal earthquake slip models for the prediction of strong ground motion. Seismol Res Lett 70:59–80. https://doi.org/10.1785/gssrl.70.1.59
43. Takahashi T, Shuto N, Imamura F, Matsutomi H (1994) The measured and computed Hokkaido Nansei-oki earthquake tsunami of 1993. In: Edge BL (ed) Coastal Engineering1994. 24th International Conference on Coastal Engineering, Kobe, October 1994. American Society of Civil Engineers, pp 886–900. https://doi.org/10.1061/9780784400890.066
44. Takahashi T, Takahashi T, Imamura F, Shuto N (1995a) Reexamination of tsunami source area of Hokkaido-Nansei-oki earthquake and tsunami. 1994 Tohoku branch of the Japan society of civil engineers technical meeting, II -60 (in Japanese)
45. Takahashi T, Takahashi T, Shuto N, Imamura F, Ortiz M (1995b) Source models for the 1993 Hokkaido Nansei-Oki earthquake tsunami. Pure Appl Geophys 144:747–767. https://doi.org/10.1007/BF00874393
46. Takemura M (1998) Scaling law for Japanese intraplate earthquakes in special relations to the surface faults and the damages. Zisin 51:211–228 (in Japanese with English abstract)
47. Tanioka Y, Satake K, Ruff L (1995) Total analysis of the 1993 Hokkaido Nanseioki earthquake using seismic wave, tsunami, and geodetic data. Geophys Res Lett 22:9–12. https://doi.org/10.1029/94GL02787
48. Usami T, Ishii H, Imamura T, Takemura M, Matsu'ura RS (2013) Materials for comprehensive list of Japanese destructive earthquakes 599–2012 [Revised 2013]. Univ Tokyo Press, Tokyo, p 694 (in Japanese)
49. Wessel P, Smith WHF (1998) New, Improved Version of Generic Mapping Tools Released. EOS Trans AGU 79(47):579

Figures

Figure 1

Epicenters of earthquakes from 1920 to 2020 with M ≥ 5.0 and shallower than 100 km by JMA catalog. Stars and circles are M ≥ 6.9 and 6.9 > M ≥ 5.0 earthquakes, respectively. Blue stars show earthquakes for which fault models are estimated from seismic analyses and offshore active faults. Red stars show earthquakes for which fault models of previous studies and offshore active faults are used. Green box in the inset map shows the area of Hokkaido and Tohoku.

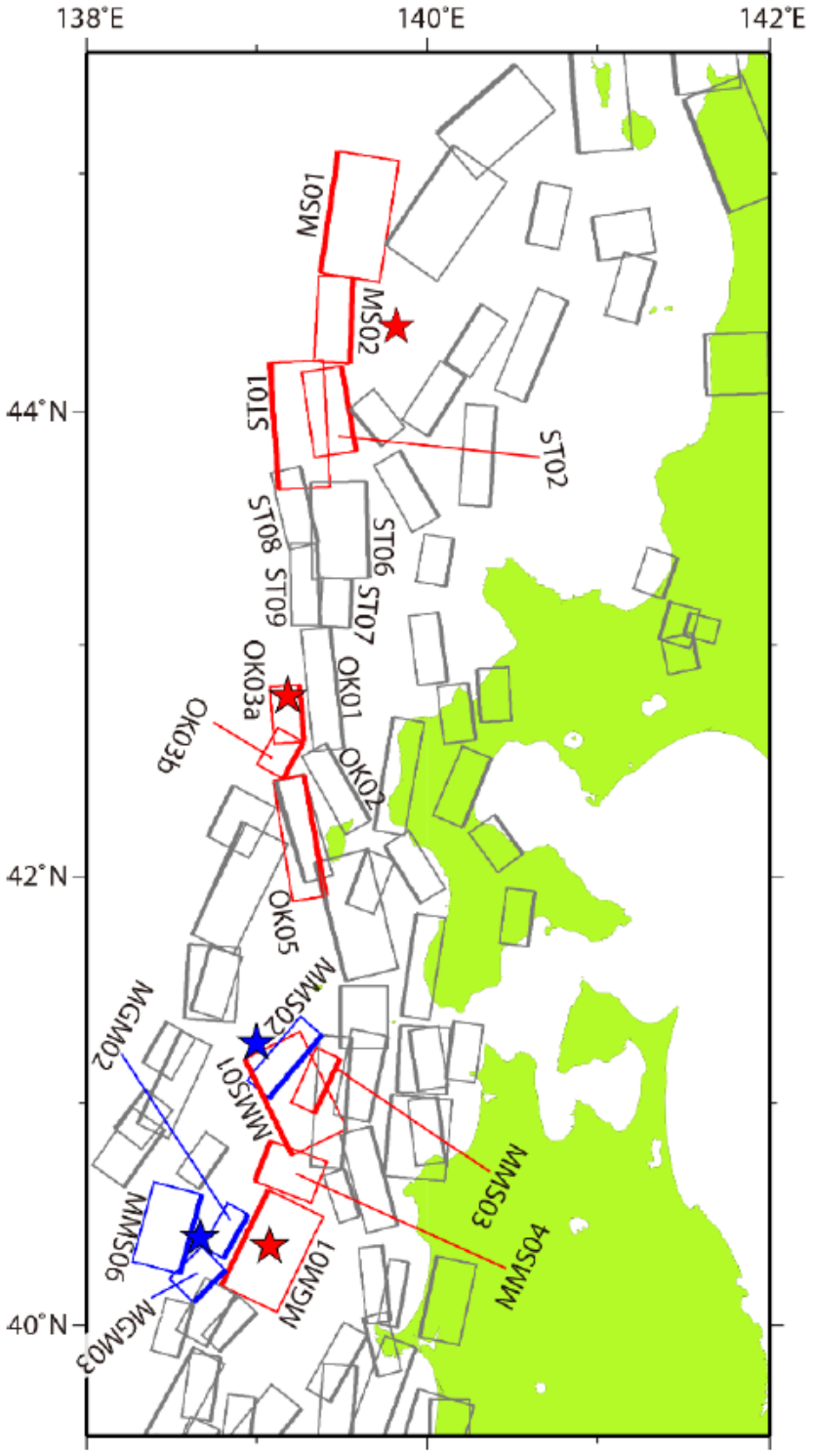

Figure 2

Offshore active faults obtained by JSPJ (2021). Red and blue stars show target earthquakes in this study.

Figure 3

Tide gauge stations where the observed tsunami waveforms were recorded. Tsunami numerical simulations were made in this region with shown bathymetry.

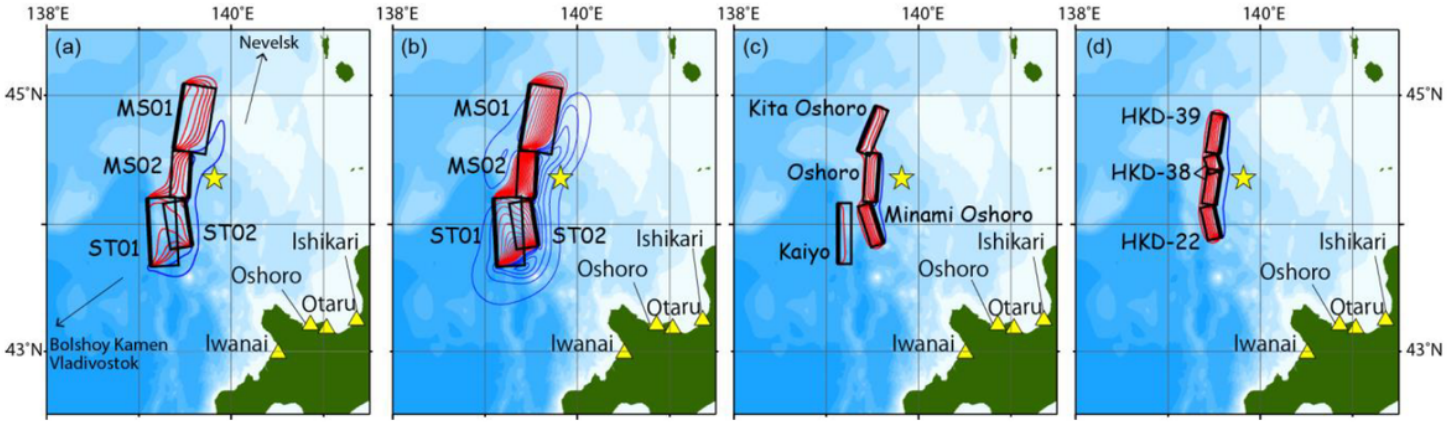

Figure 4

Seafloor displacements for the 1940 off Shakotan Peninsula earthquake (MJMA 7.5) calculated from (a) Model Ar, (b) Model At, (c) Okamura et al. (2005), and (d) Ohsumi and Fujiwara (2017). Counter interval is 20 cm. Red and blue curves show uplift and subsidence, respectively. Star shows the epicenter from JMA catalog. Yellow triangles are tide gauge stations. Fault names in the referenced papers are added in (c) and (d).

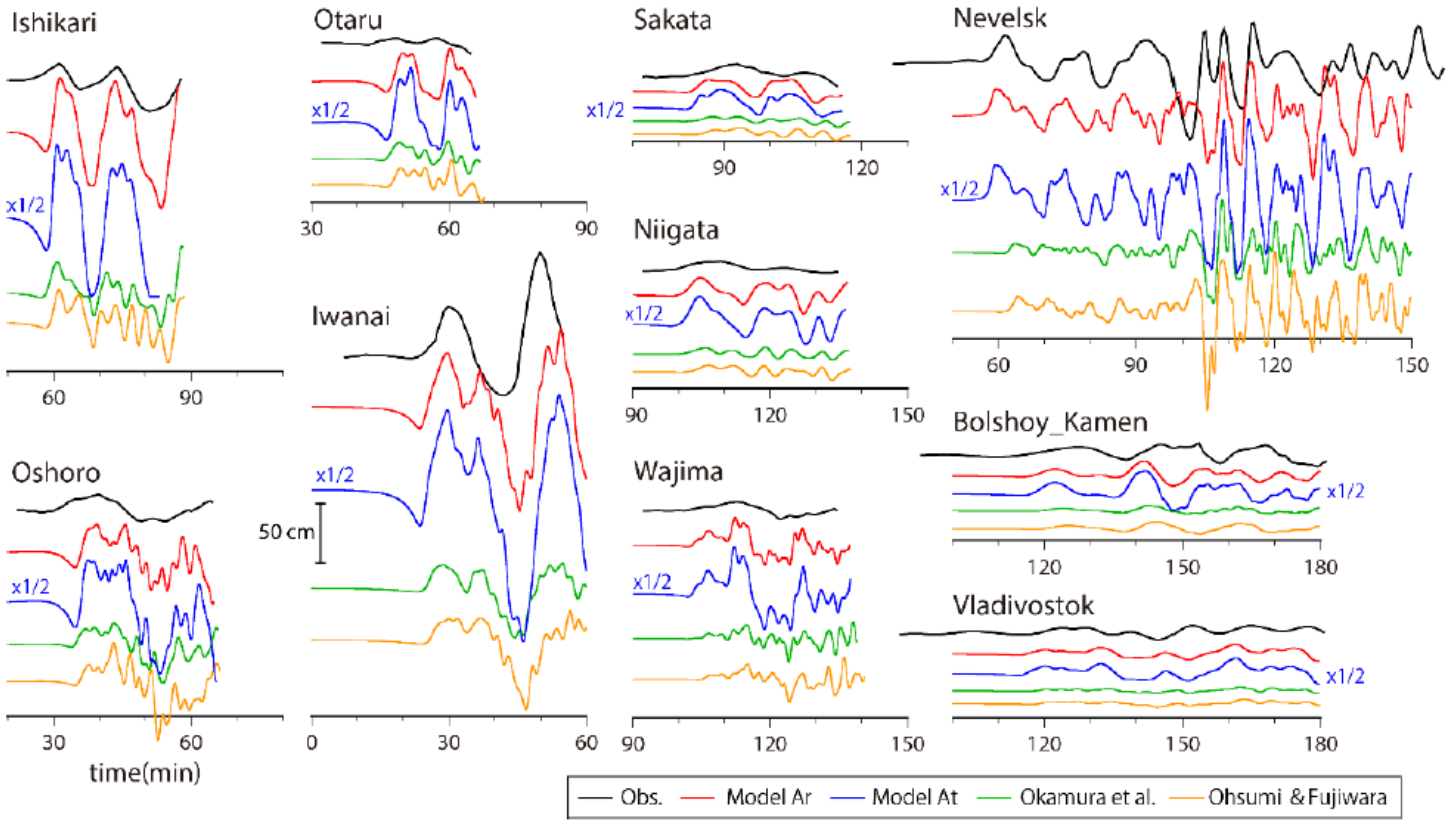

Figure 5

Comparison between the observed and calculated tsunami waveforms for the 1940 off Shakotan Peninsula earthquake.

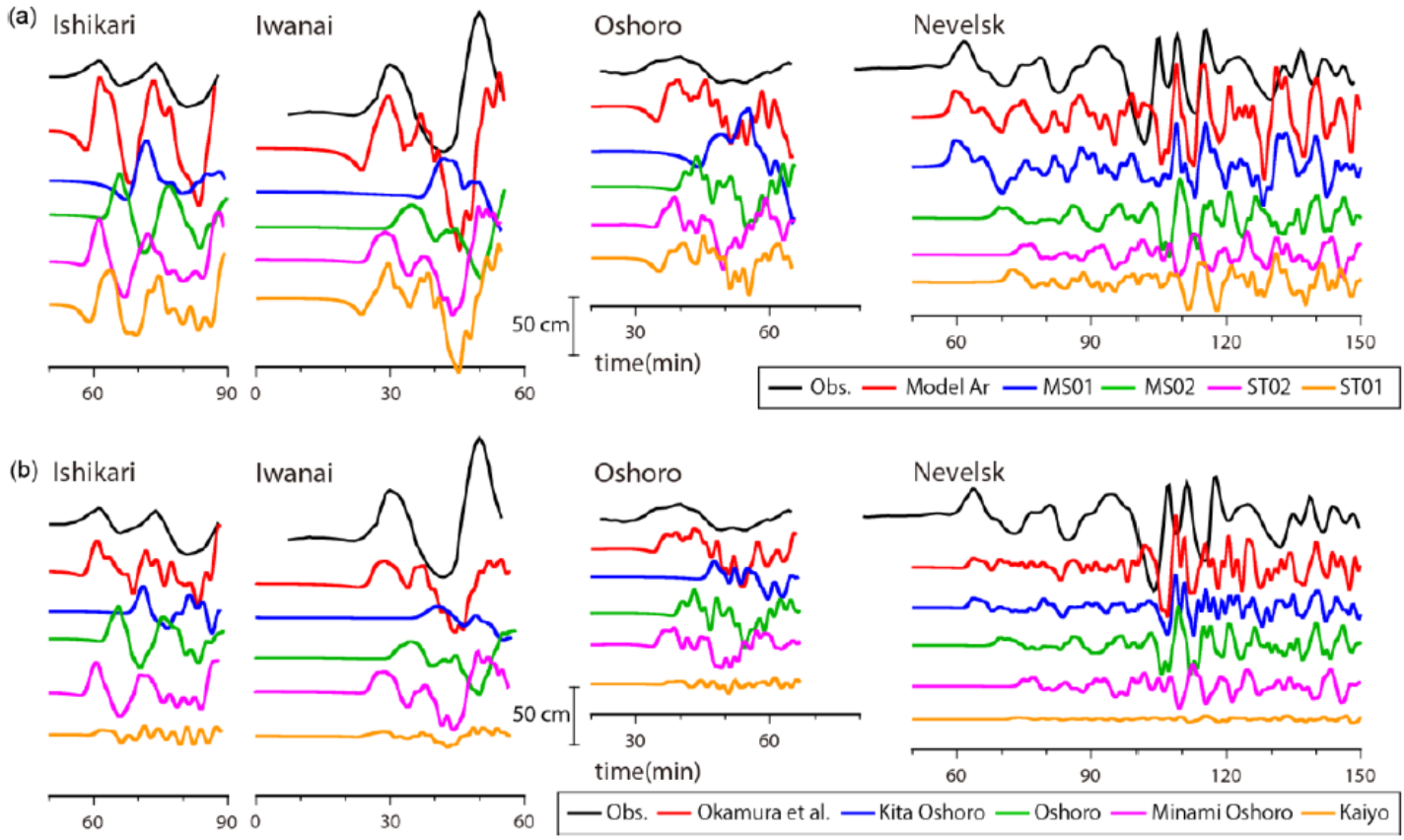

Figure 6

Comparison between the observed and calculated waveforms from each subfault for (a) Model Ar and (b) Okamura et al. (2005) for the 1940 off Shakotan Peninsula earthquake.

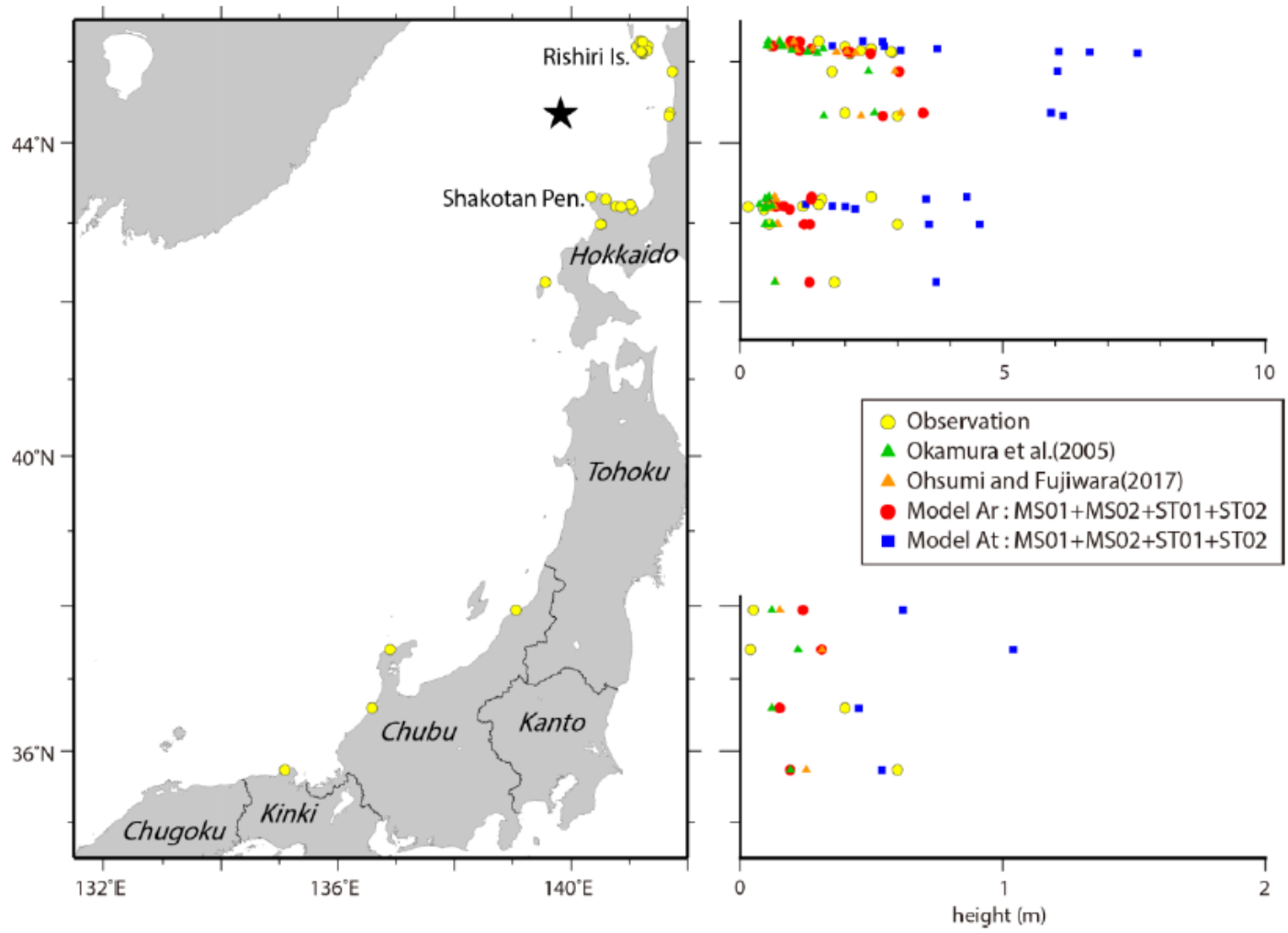

Figure 7

Comparison between the observed and calculated coastal tsunami heights for the 1940 off Shakotan Peninsula earthquake.

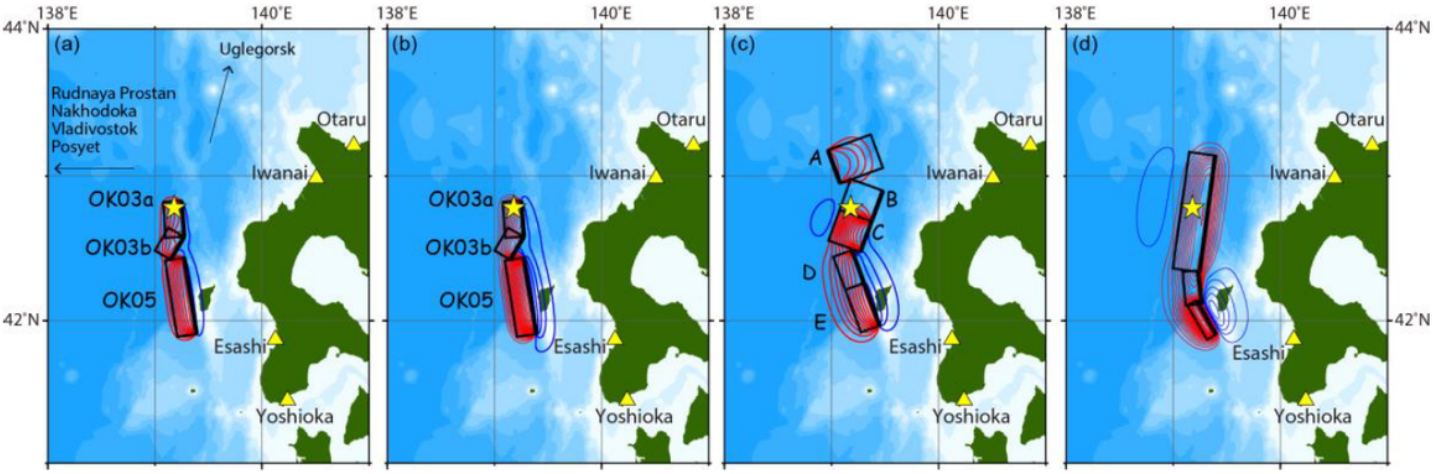

Figure 8

Seafloor displacements for the 1993 off the southwest coast of Hokkaido earthquake (MJMA 7.8) calculated from (a) Model Ar, (b) Model At, (c) Tanioka et al. (1995), and (d) Takahashi et al. (1995a). Counter interval is 20 cm. Red and blue curves show uplift and subsidence, respectively. Star shows the epicenter from JMA catalog. Fault names used in the referenced paper are added in (c).

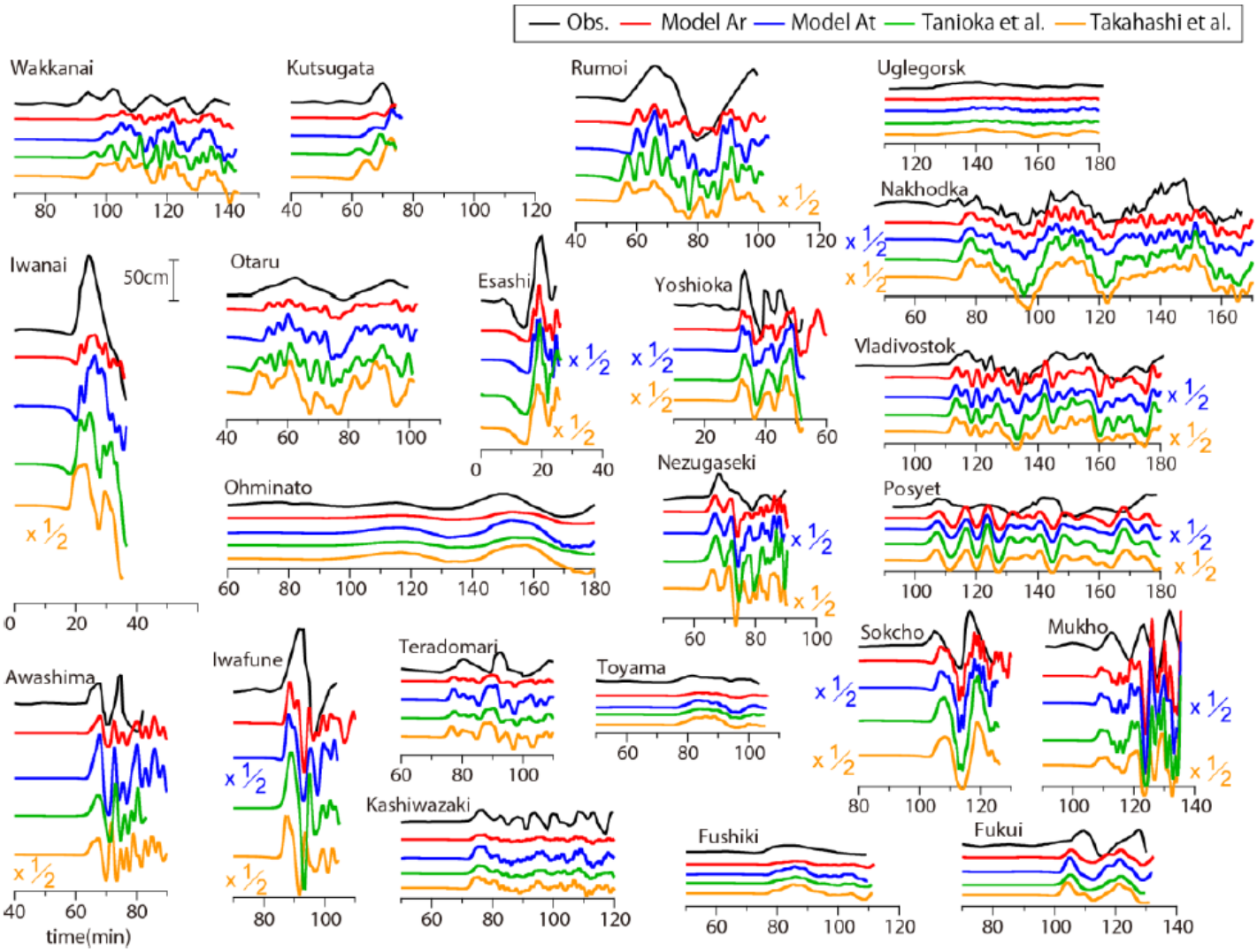

Figure 9

Comparison between the observed and calculated tsunami waveforms for the 1993 off the southwest coast of Hokkaido earthquake.

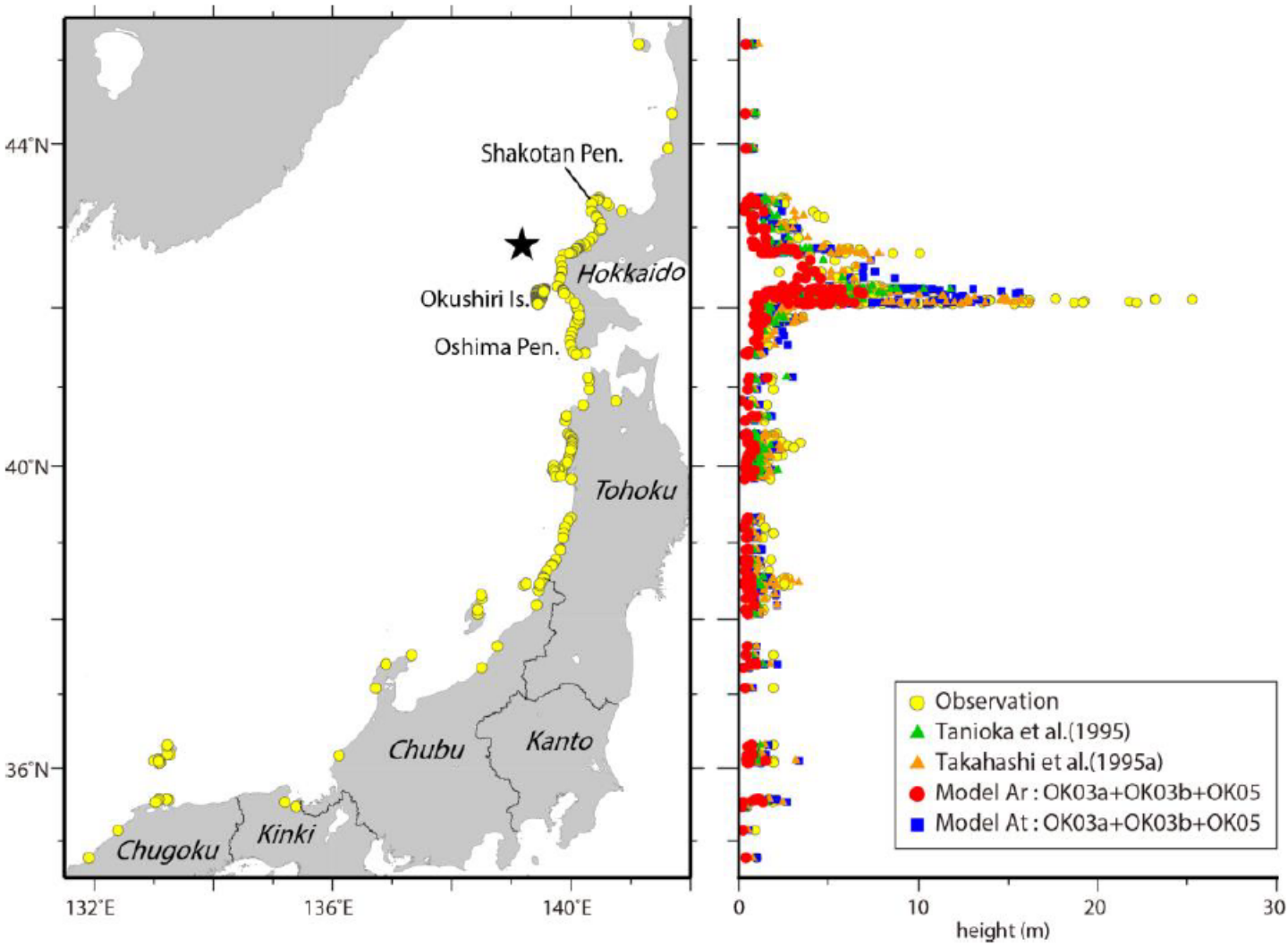

Figure 10

Comparison between the observed and calculated coastal tsunami heights for the 1993 off the southwest coast of Hokkaido earthquake.

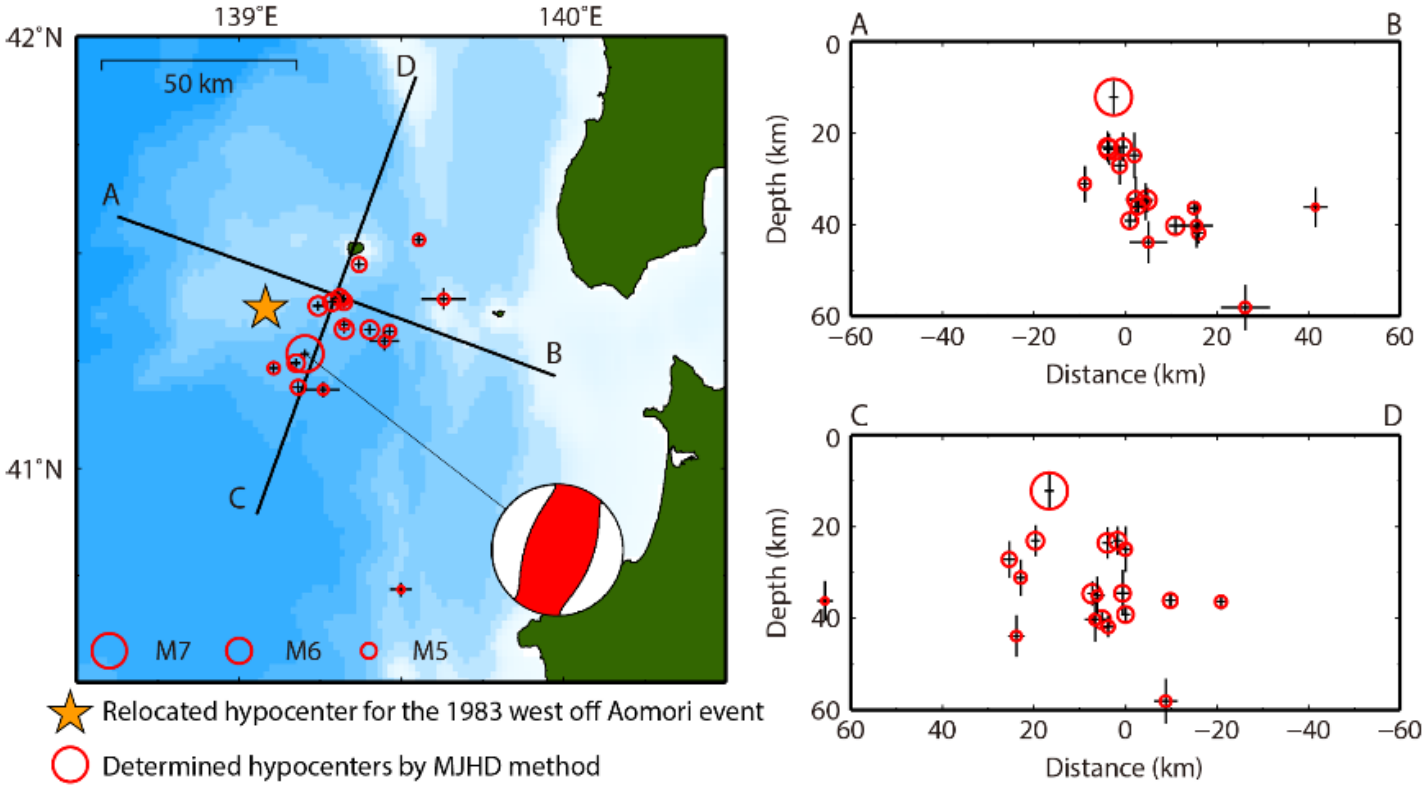

Figure 11

Relocated hypocenter by HYPOSAT for the 1983 west off Aomori earthquake (MJMA 7.1) and its relative hypocenter locations with aftershocks by MJHD method.

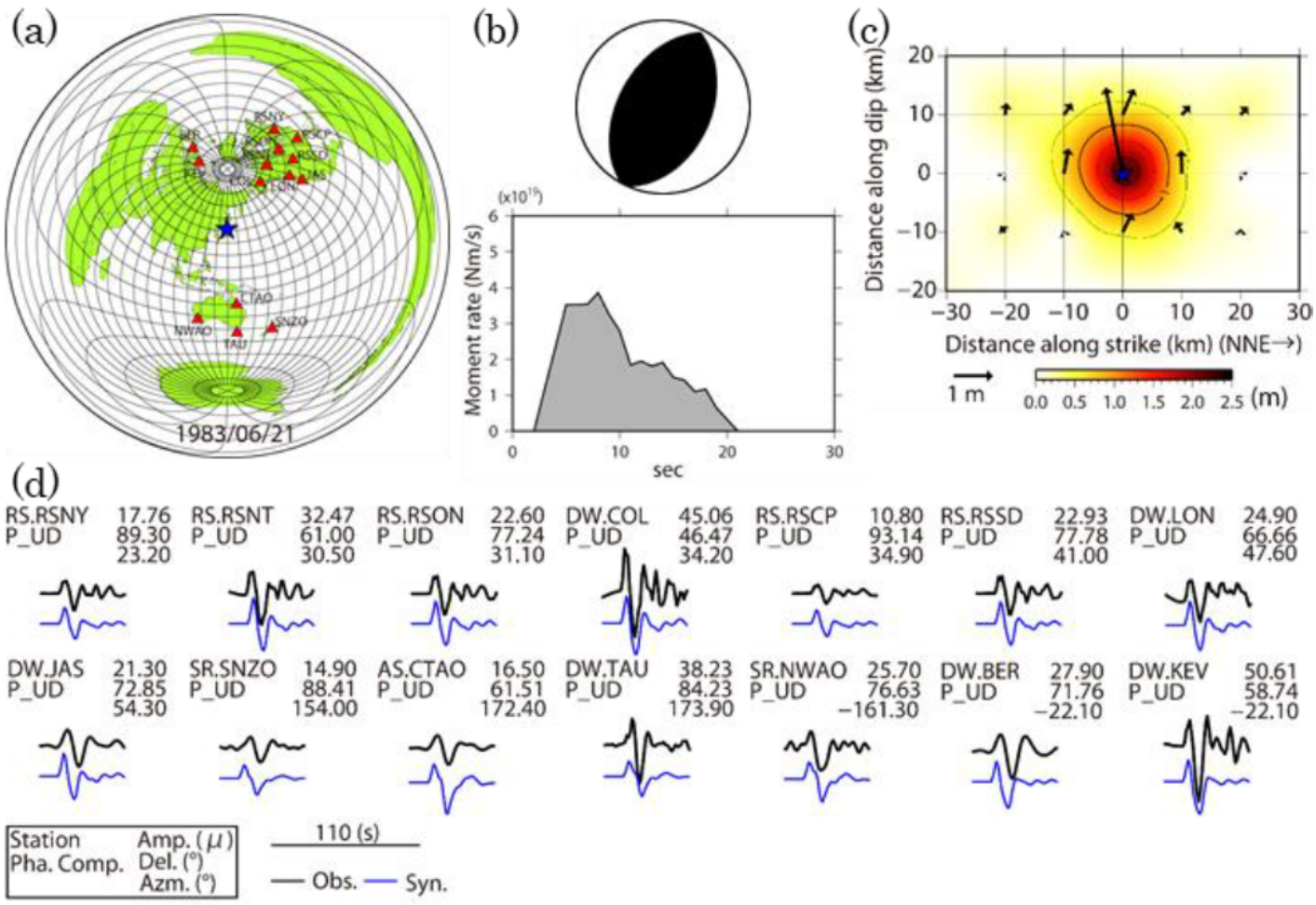

Figure 12

Result of teleseismic waveform inversion for the 1983 west off Aomori earthquake. (a) station map, (b) fault mechanism and source time function, (c) slip distribution, and (d) comparison between the observed and synthetic waveforms.

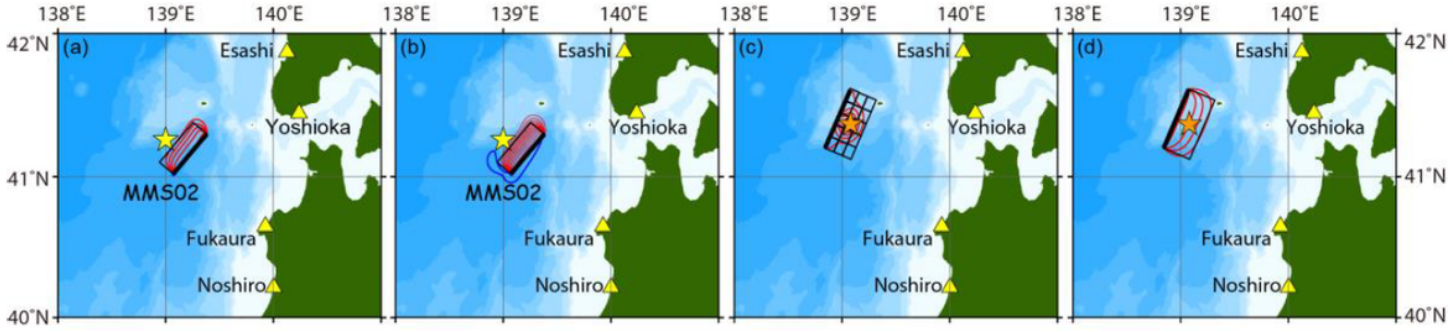

Figure 13

Seafloor displacements for the 1983 west off Aomori earthquake (MJMA 7.1) calculated from (a) Model Ar, (b) Model At, (c) seismic inversion model, and (d) modified model with uniform slip. Counter interval is

10 cm. Red and blue curves show uplift and subsidence, respectively. Yellow star shows the epicenter from JMA catalog. Orange star shows the epicenter relocated by HYPOSAT. Yellow triangles are tide gauge stations.

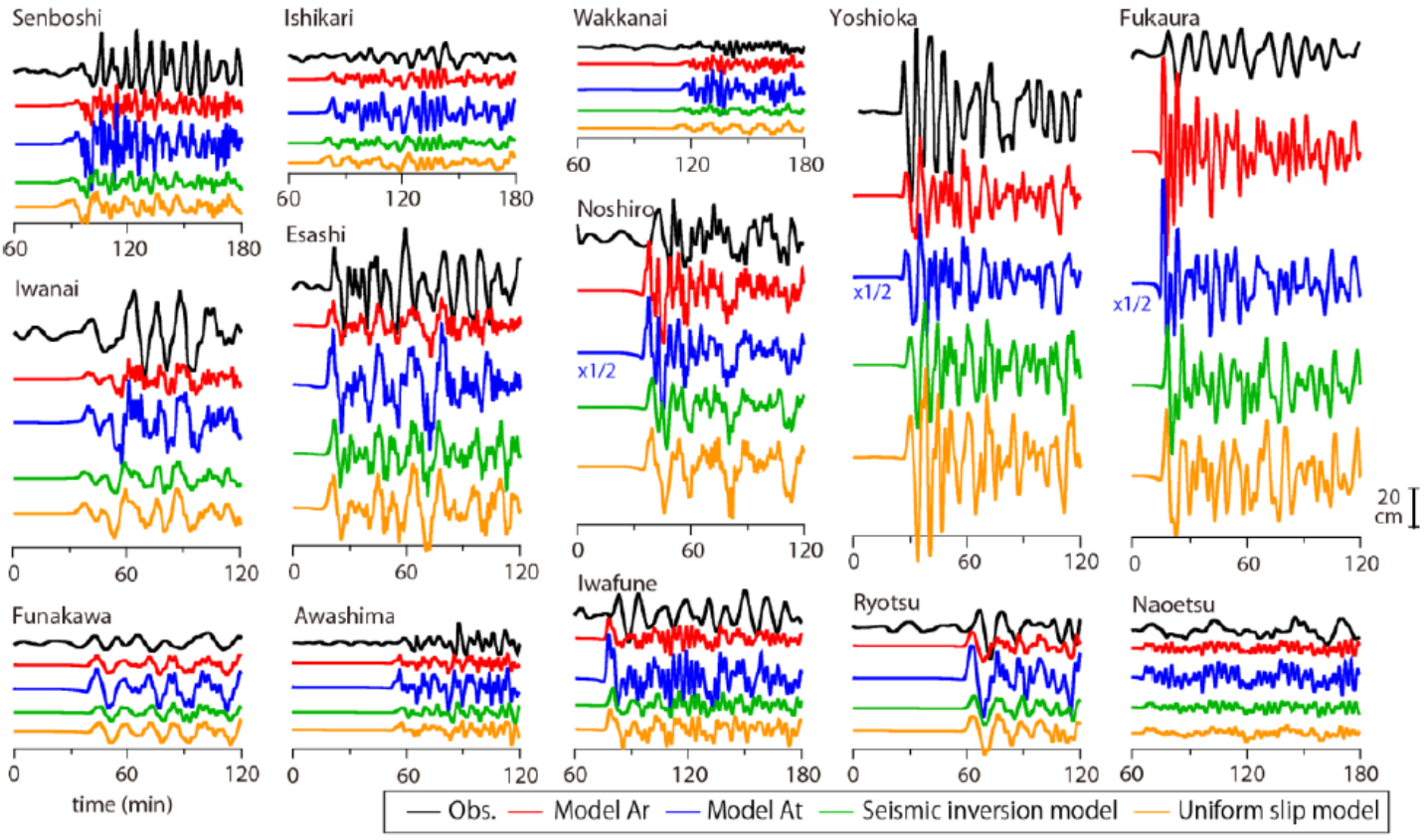

Figure 14

Comparison between the observed and calculated tsunami waveforms for the 1983 west off Aomori earthquake.

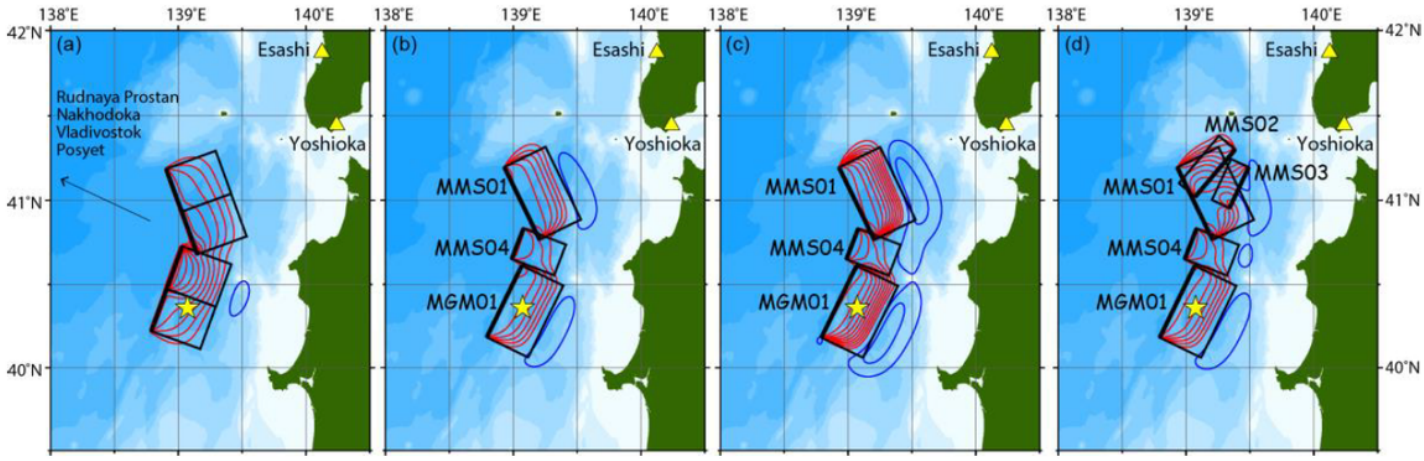

Figure 15

Seafloor displacements for the 1983 Central Sea of Japan earthquake (MJMA 7.7) calculated from (a) Satake (1989), (b) Model Ar, (c) Model At, and (d) Model Br. Counter interval is 20 cm. Red and blue curves show uplift and subsidence, respectively. Yellow star shows the epicenter from JMA catalog. Yellow triangles are tide gauge stations.

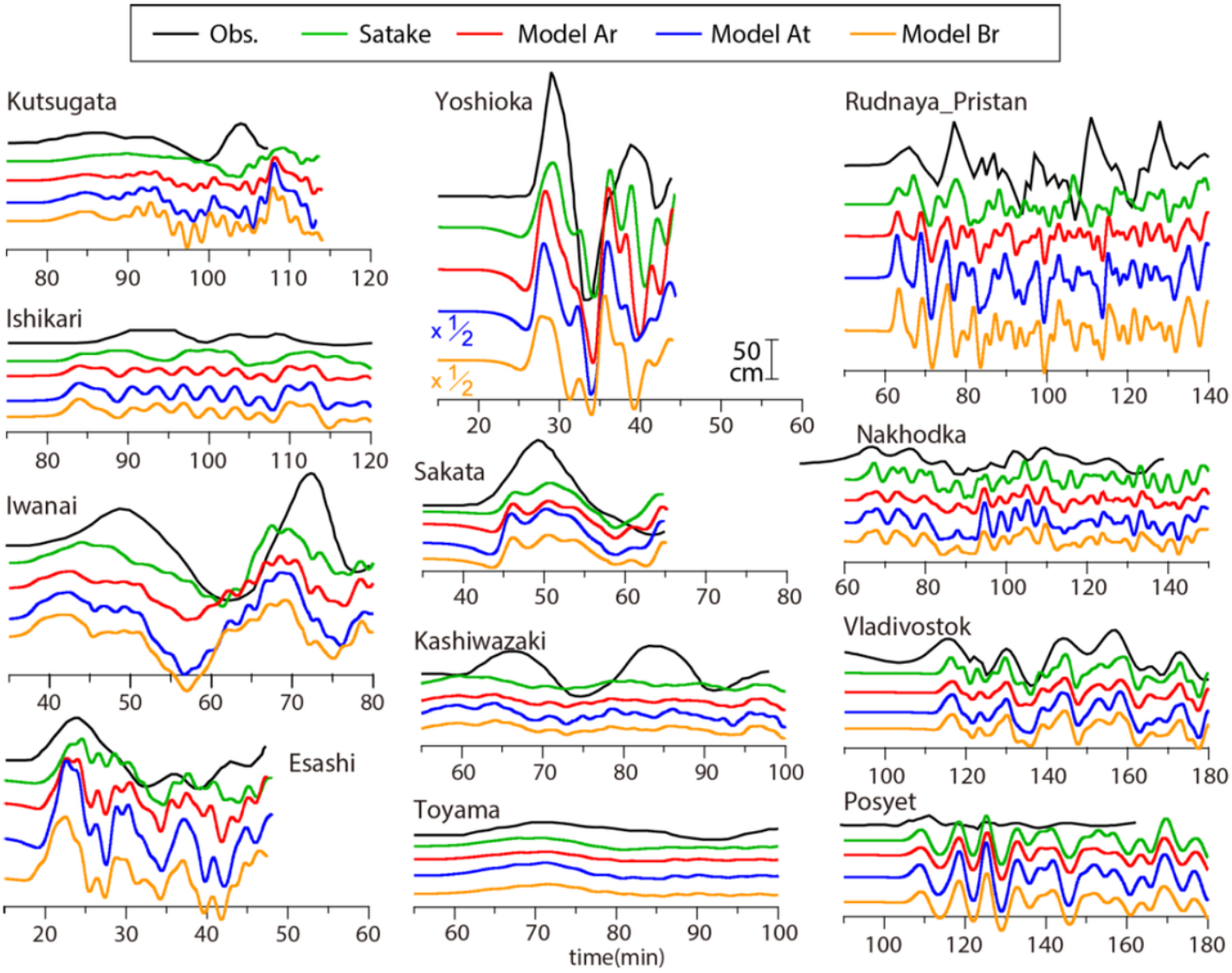

Figure 16

Comparison between the observed and calculated tsunami waveforms for the 1983 Central Sea of Japan earthquake.

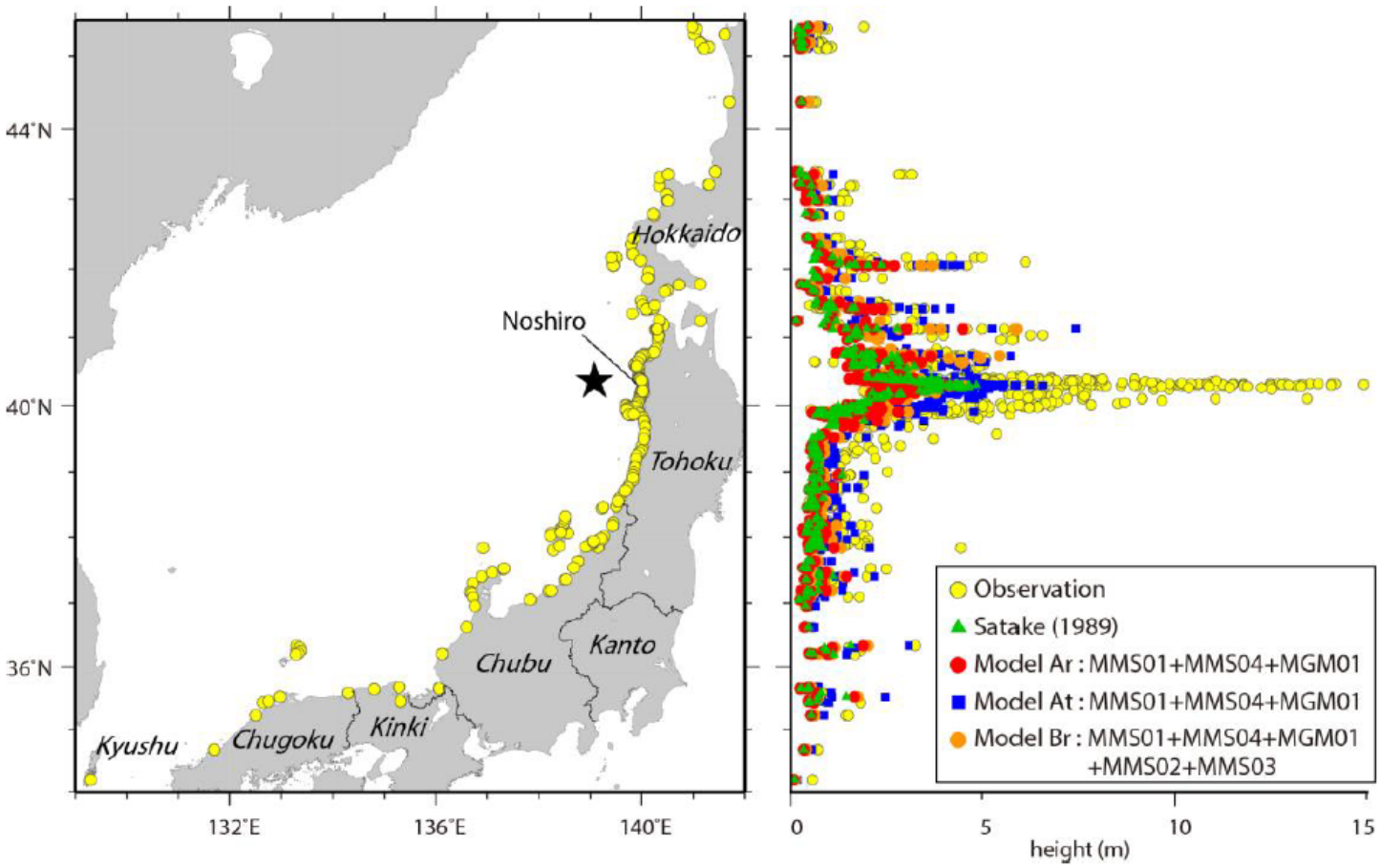

Figure 17

Comparison between the observed and calculated coastal tsunami heights for the 1983 Central Sea of Japan earthquake.

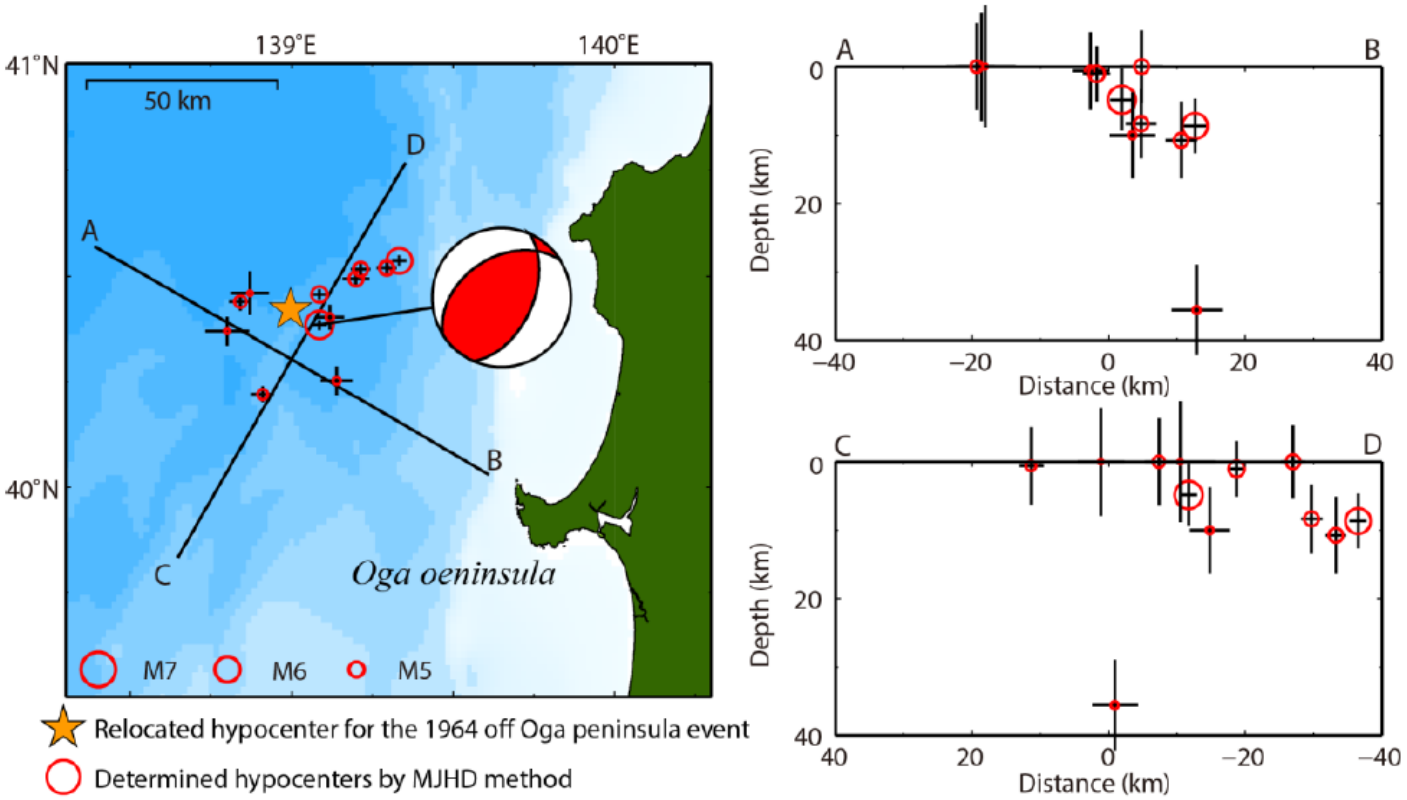

Figure 18

Relocated hypocenter for the 1964 off Oga Peninsula earthquake (MJMA 6.9) and its relative hypocenter locations with aftershocks by the MJHD method.

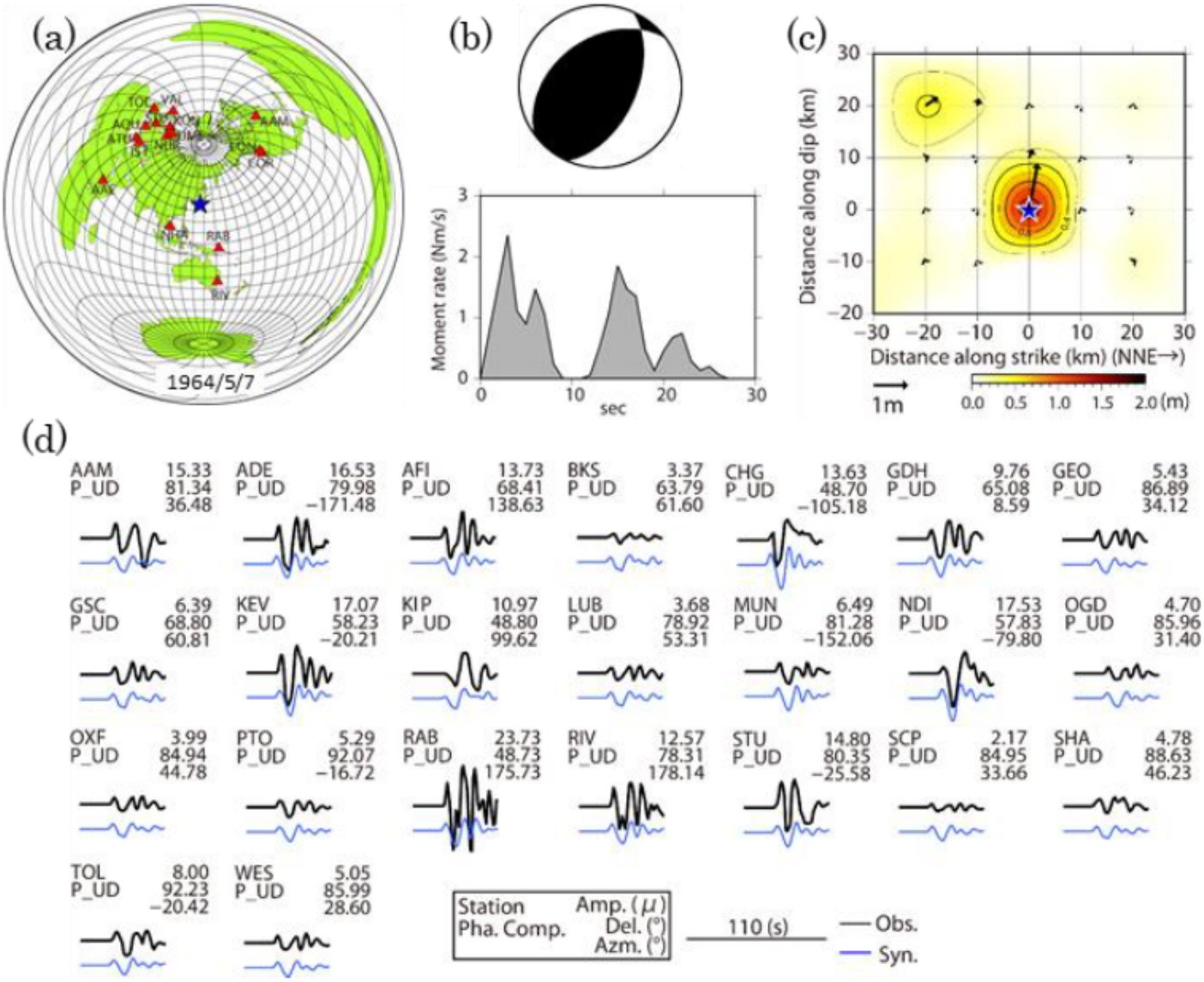

Figure 19

Result of teleseismic waveform inversion for the 1964 off Oga Peninsula earthquake. (a) station map, (b) fault mechanism and source time function, (c) slip distribution, and (d) comparison between observed and synthetic waveforms.

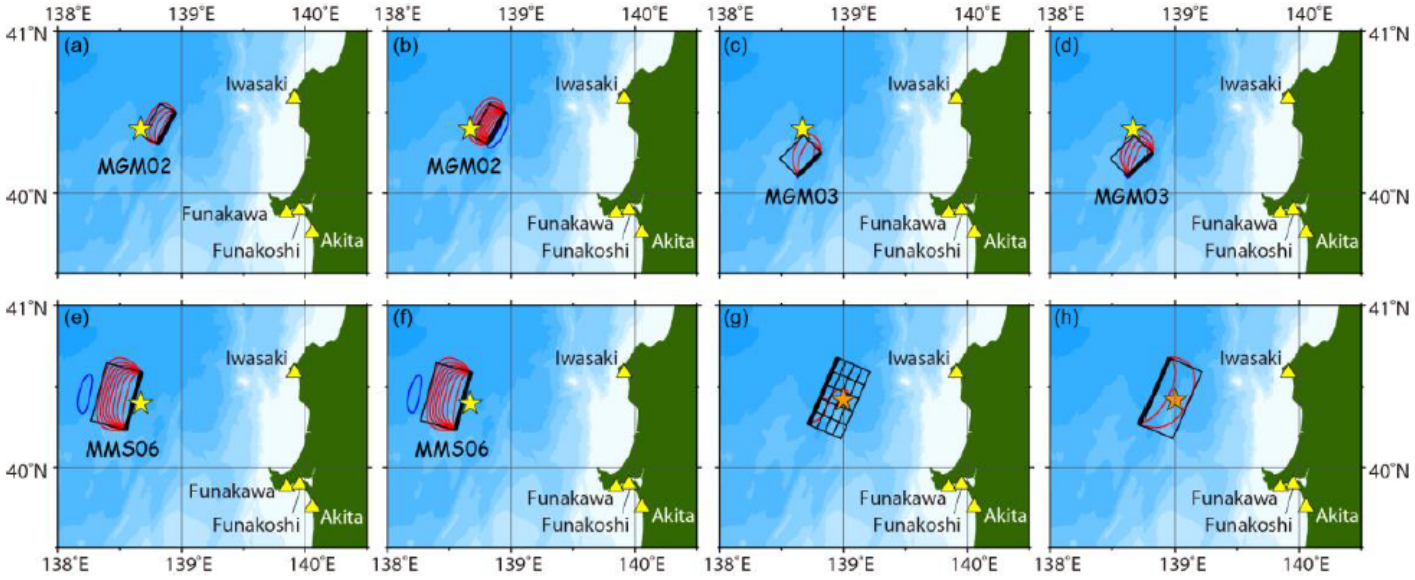

Figure 20

Seafloor displacements for the 1964 off Oga Peninsula earthquake (MJMA 6.9) calculated from (a) Model Ar, (b) Model At, (c) Model Br, (d) Model Bt, (e) Model Cr, (f) Model Ct, (g) seismic inversion model, and (h) modified model with uniform slip. Counter interval is 10 cm. Red and blue curves show uplift and subsidence, respectively. Yellow star shows the epicenter from JMA catalog. Orange star shows the epicenter redetermined by HYPOSAT. Yellow triangles are tide gauge stations.

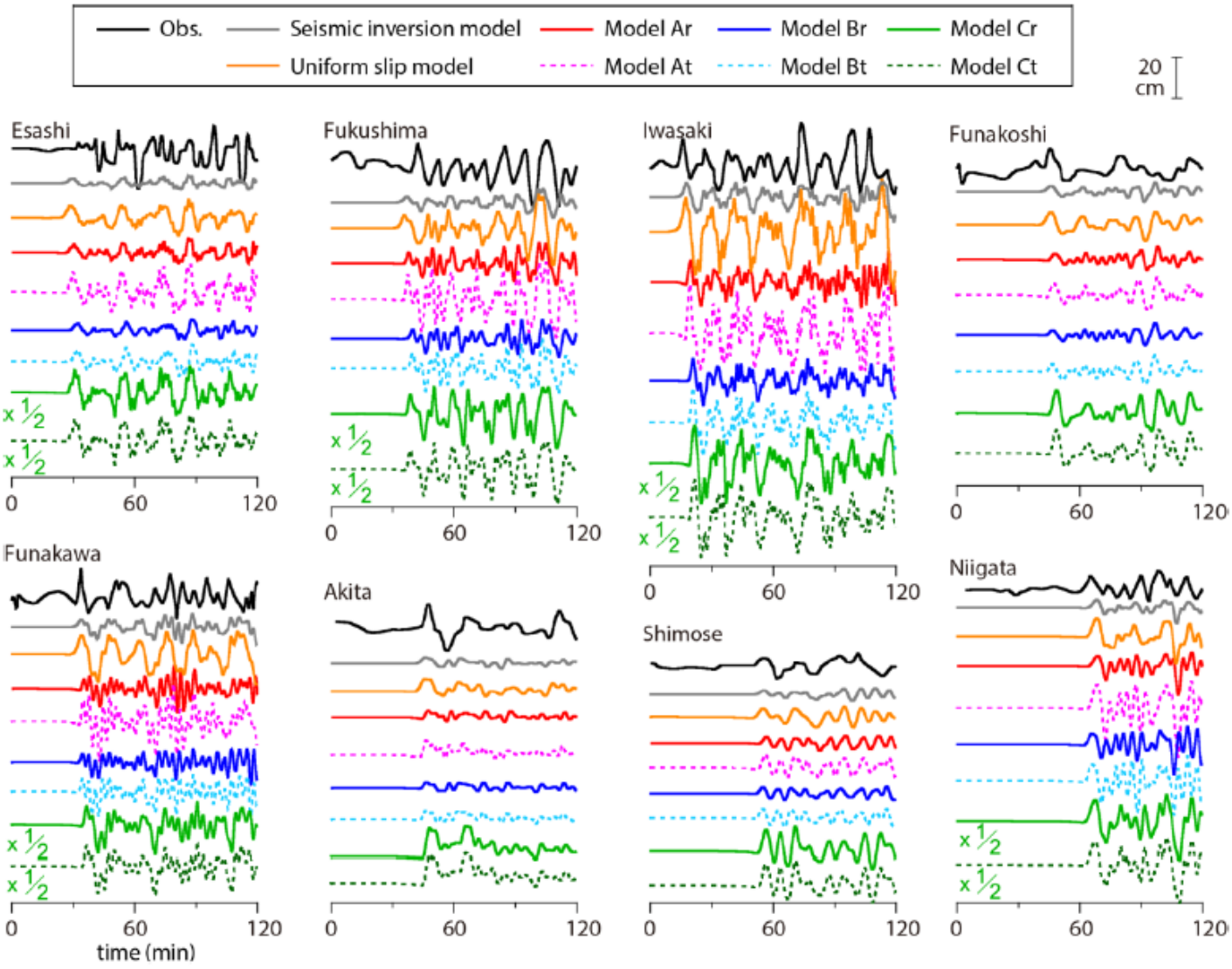

Figure 21

Comparison between the observed and calculated tsunami waveforms for the 1964 off Oga Peninsula earthquake.

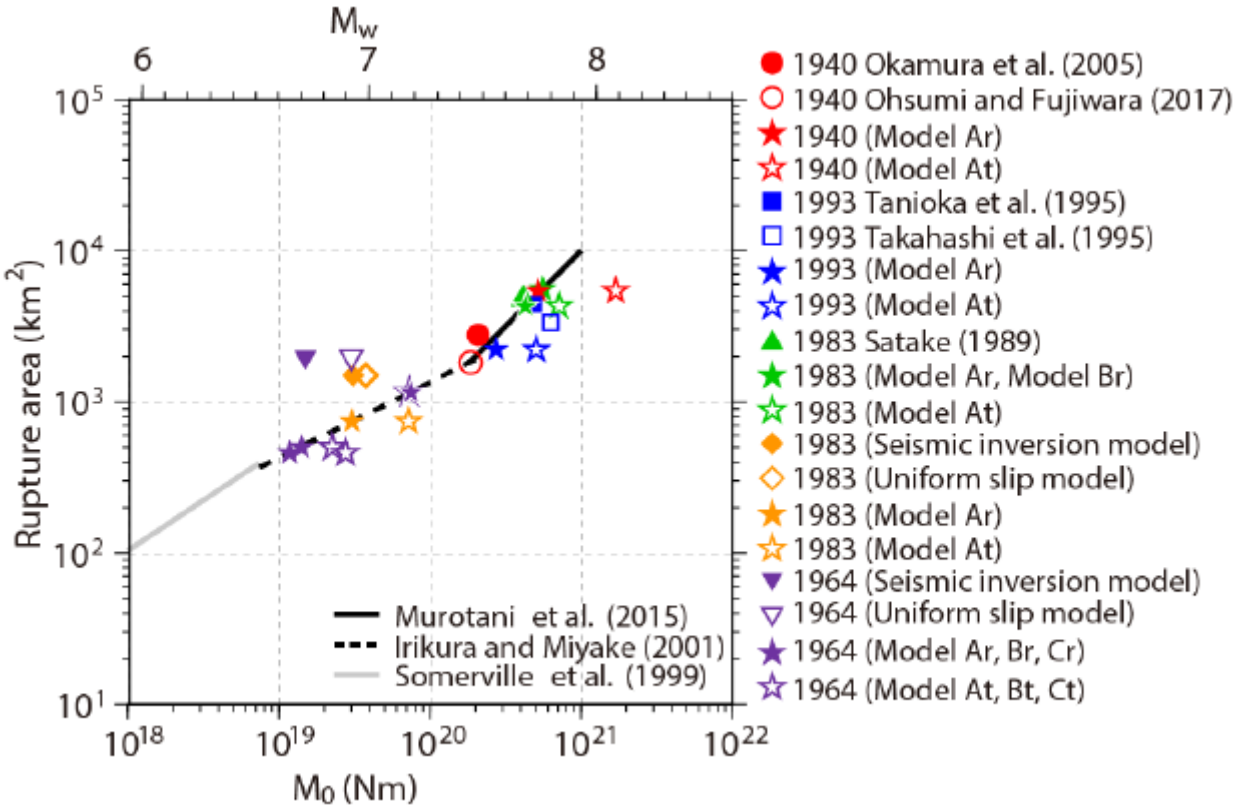

Figure 22

Relationship between seismic moment and rupture area for fault models of each earthquake used in this study.

Supplementary Files

This is a list of supplementary files associated with this preprint. Click to download.

- Additionalfile1.docx
- abstractimage.png